

$B \rightarrow D^* \pi^+ \pi^- \pi^- \pi^0, D^{(*)} \omega \pi^-$ and the Observation of a
Wide $1^- \omega \pi^-$ Enhancement at 1418 MeV

CLEO Collaboration

June 15, 2000

Abstract

We report on the observation of $B \rightarrow D^* \pi^+ \pi^- \pi^- \pi^0$ decays. The branching ratios for D^{*+} and D^{*0} are $(1.72 \pm 0.14 \pm 0.24)\%$ and $(1.80 \pm 0.24 \pm 0.25)\%$, respectively. Each final state has a $D^* \omega \pi^-$ component, with branching ratios $(0.29 \pm 0.03 \pm 0.04)\%$ and $(0.45 \pm 0.10 \pm 0.07)\%$ for the D^{*+} and D^{*0} modes, respectively. We also observe $B \rightarrow D \omega \pi^-$ decays. The branching ratios for D^+ and D^0 are $(0.28 \pm 0.05 \pm 0.03)\%$ and $(0.41 \pm 0.07 \pm 0.04)\%$, respectively. The $\omega \pi^-$ appears to come from the decay of a wide 1^- resonance. A fit to a Breit-Wigner shape gives a mass of $1418 \pm 26 \pm 19$ MeV and width of $388 \pm 44 \pm 32$ MeV. We identify this object as the $\rho(1450)$ or ρ' .

.....
Submitted to XXXth International Conference on High Energy Physics, July 2000, Osaka,
Japan

M. Artuso,¹ R. Ayad,¹ C. Boulahouache,¹ K. Bukin,¹ E. Dambasuren,¹ S. Karamov,¹
 G. Majumder,¹ G. C. Moneti,¹ R. Mountain,¹ S. Schuh,¹ T. Skwarnicki,¹ S. Stone,¹
 G. Viehhauser,¹ J.C. Wang,¹ A. Wolf,¹ J. Wu,¹ S. Kopp,² A. H. Mahmood,³ S. E. Csorna,⁴
 I. Danko,⁴ K. W. McLean,⁴ Sz. Márka,⁴ Z. Xu,⁴ R. Godang,⁵ K. Kinoshita,^{5,1} I. C. Lai,⁵
 S. Schrenk,⁵ G. Bonvicini,⁶ D. Cinabro,⁶ S. McGee,⁶ L. P. Perera,⁶ G. J. Zhou,⁶
 E. Lipeles,⁷ S. P. Pappas,⁷ M. Schmidtler,⁷ A. Shapiro,⁷ W. M. Sun,⁷ A. J. Weinstein,⁷
 F. Würthwein,^{7,2} D. E. Jaffe,⁸ G. Masek,⁸ H. P. Paar,⁸ E. M. Potter,⁸ S. Prell,⁸
 V. Sharma,⁸ D. M. Asner,⁹ A. Eppich,⁹ T. S. Hill,⁹ R. J. Morrison,⁹ R. A. Briere,¹⁰
 G. P. Chen,¹⁰ T. Ferguson,¹⁰ B. H. Behrens,¹¹ W. T. Ford,¹¹ A. Gribsan,¹¹ J. Roy,¹¹
 J. G. Smith,¹¹ J. P. Alexander,¹² R. Baker,¹² C. Bebek,¹² B. E. Berger,¹² K. Berkelman,¹²
 F. Blanc,¹² V. Boisvert,¹² D. G. Cassel,¹² M. Dickson,¹² P. S. Drell,¹² K. M. Ecklund,¹²
 R. Ehrlich,¹² A. D. Foland,¹² P. Gaidarev,¹² L. Gibbons,¹² B. Gittelman,¹² S. W. Gray,¹²
 D. L. Hartill,¹² B. K. Heltsley,¹² P. I. Hopman,¹² C. D. Jones,¹² D. L. Kreinick,¹²
 M. Lohner,¹² A. Magerkurth,¹² T. O. Meyer,¹² N. B. Mistry,¹² E. Nordberg,¹²
 J. R. Patterson,¹² D. Peterson,¹² D. Riley,¹² J. G. Thayer,¹² D. Urner,¹²
 B. Valant-Spaight,¹² A. Warburton,¹² P. Avery,¹³ C. Prescott,¹³ A. I. Rubiera,¹³
 J. Yelton,¹³ J. Zheng,¹³ G. Brandenburg,¹⁴ A. Ershov,¹⁴ Y. S. Gao,¹⁴ D. Y.-J. Kim,¹⁴
 R. Wilson,¹⁴ T. E. Browder,¹⁵ Y. Li,¹⁵ J. L. Rodriguez,¹⁵ H. Yamamoto,¹⁵ T. Bergfeld,¹⁶
 B. I. Eisenstein,¹⁶ J. Ernst,¹⁶ G. E. Gladding,¹⁶ G. D. Gollin,¹⁶ R. M. Hans,¹⁶ E. Johnson,¹⁶
 I. Karliner,¹⁶ M. A. Marsh,¹⁶ M. Palmer,¹⁶ C. Plager,¹⁶ C. Sedlack,¹⁶ M. Selen,¹⁶
 J. J. Thaler,¹⁶ J. Williams,¹⁶ K. W. Edwards,¹⁷ R. Janicek,¹⁸ P. M. Patel,¹⁸ A. J. Sadoff,¹⁹
 R. Ammar,²⁰ A. Bean,²⁰ D. Besson,²⁰ R. Davis,²⁰ N. Kwak,²⁰ X. Zhao,²⁰ S. Anderson,²¹
 V. V. Frolov,²¹ Y. Kubota,²¹ S. J. Lee,²¹ R. Mahapatra,²¹ J. J. O'Neill,²¹ R. Poling,²¹
 T. Riehle,²¹ A. Smith,²¹ C. J. Stepaniak,²¹ J. Urheim,²¹ S. Ahmed,²² M. S. Alam,²²
 S. B. Athar,²² L. Jian,²² L. Ling,²² M. Saleem,²² S. Timm,²² F. Wappler,²² A. Anastassov,²³
 J. E. Duboscq,²³ E. Eckhart,²³ K. K. Gan,²³ C. Gwon,²³ T. Hart,²³ K. Honscheid,²³
 D. Hufnagel,²³ H. Kagan,²³ R. Kass,²³ T. K. Pedlar,²³ H. Schwarthoff,²³ J. B. Thayer,²³
 E. von Toerne,²³ M. M. Zoeller,²³ S. J. Richichi,²⁴ H. Severini,²⁴ P. Skubic,²⁴ A. Undrus,²⁴
 S. Chen,²⁵ J. Fast,²⁵ J. W. Hinson,²⁵ J. Lee,²⁵ D. H. Miller,²⁵ E. I. Shibata,²⁵
 I. P. J. Shipsey,²⁵ V. Pavlunin,²⁵ D. Cronin-Hennessy,²⁶ A.L. Lyon,²⁶ E. H. Thorndike,²⁶
 C. P. Jessop,²⁷ H. Marsiske,²⁷ M. L. Perl,²⁷ V. Savinov,²⁷ X. Zhou,²⁷ T. E. Coan,²⁸
 V. Fadeyev,²⁸ Y. Maravin,²⁸ I. Narsky,²⁸ R. Stroynowski,²⁸ J. Ye,²⁸ and T. Wlodek²⁸

¹Syracuse University, Syracuse, New York 13244

²University of Texas, Austin, TX 78712

³University of Texas - Pan American, Edinburg, TX 78539

⁴Vanderbilt University, Nashville, Tennessee 37235

⁵Virginia Polytechnic Institute and State University, Blacksburg, Virginia 24061

⁶Wayne State University, Detroit, Michigan 48202

⁷California Institute of Technology, Pasadena, California 91125

⁸University of California, San Diego, La Jolla, California 92093

⁹University of California, Santa Barbara, California 93106

¹⁰Carnegie Mellon University, Pittsburgh, Pennsylvania 15213

¹Permanent address: University of Cincinnati, Cincinnati, OH 45221

²Permanent address: Massachusetts Institute of Technology, Cambridge, MA 02139.

- ¹¹University of Colorado, Boulder, Colorado 80309-0390
¹²Cornell University, Ithaca, New York 14853
¹³University of Florida, Gainesville, Florida 32611
¹⁴Harvard University, Cambridge, Massachusetts 02138
¹⁵University of Hawaii at Manoa, Honolulu, Hawaii 96822
¹⁶University of Illinois, Urbana-Champaign, Illinois 61801
¹⁷Carleton University, Ottawa, Ontario, Canada K1S 5B6
and the Institute of Particle Physics, Canada
¹⁸McGill University, Montréal, Québec, Canada H3A 2T8
and the Institute of Particle Physics, Canada
¹⁹Ithaca College, Ithaca, New York 14850
²⁰University of Kansas, Lawrence, Kansas 66045
²¹University of Minnesota, Minneapolis, Minnesota 55455
²²State University of New York at Albany, Albany, New York 12222
²³Ohio State University, Columbus, Ohio 43210
²⁴University of Oklahoma, Norman, Oklahoma 73019
²⁵Purdue University, West Lafayette, Indiana 47907
²⁶University of Rochester, Rochester, New York 14627
²⁷Stanford Linear Accelerator Center, Stanford University, Stanford, California 94309
²⁸Southern Methodist University, Dallas, Texas 75275

1 Introduction

Understanding hadronic decays of the B is crucial to insuring that decay modes used for measurement of CP violation truly reflect the underlying quark decay mechanisms expected theoretically.

Currently, measured exclusive branching ratios for hadronic B decays total only a small fraction of the hadronic width. The semileptonic branching ratio for $B \rightarrow X e^- \nu$, $X \mu^- \nu$, and $X \tau^- \nu$ totals approximately 25% [1]. The measured hadronic decay modes for the \overline{B}^0 including $D^+(n\pi^-)$, $D^{*+}(n\pi^-)$, where $3 \geq n \geq 1$, $D^{(*)}D_s^{-(*)}$, and J/ψ exclusive totals only about 10% [1]. (The B^- modes total about 12%.) Thus our understanding of hadronic B decay modes is not yet well based in data.

It is also interesting to note that the average charged multiplicity in a hadronic B^0 decay is 5.3 ± 0.1 [2]. Since this multiplicity contains contributions from the D^+ or D^{*+} normally present in \overline{B}^0 decay, we expect a sizeable, approximately several percent, decay rate into final states with four pions [3]. The seen $D^{(*)}(n\pi)^-$ final states for $n \leq 3$ are consistent with being quasi-two-body final states. For n of two the ρ^- dominates, while for n of three the a_1^- dominates [4]. These decays appear to occur from a simple spectator mechanism where the virtual W^- materializes as a single hadron: π^- , ρ^- or a_1^- .

In this paper we investigate final states for n of 4. We will show a large signal for the $D^{*+}\pi^+\pi^-\pi^-\pi^0$ final state in section 3. In section 4 we will show that a substantial fraction, $\sim 20\%$ arise from $D^{*+}\omega\pi^-$ decays and that the $\omega\pi^-$ mass distribution has a resonant structure around 1.42 GeV with a width of about 0.4 GeV. In section 5, the similar conclusions are drawn about the $D^{*0}\pi^+\pi^-\pi^-\pi^0$ final state. The same structure is shown to exist in $D\omega\pi^-$ final states (section 7) and we will use these events to show in section 7.6 that the spin-parity is most likely 1^- . This state is identified as the ρ' , also sometimes called the $\rho(1450)$. Other resonant substructure is searched for, but not found (section 9). Finally we summarize our findings and compare with the predictions of factorization and other models in section 10.

The data sample consists of 9.0 fb^{-1} of integrated luminosity taken with the CLEO II and II.V detectors [5] using the CESR e^+e^- storage ring on the peak of the $\Upsilon(4S)$ resonance and 4.4 fb^{-1} in the continuum at 60 MeV less center-of-mass energy. The sample contains 19.4 million B mesons.

2 Common Selection Criteria

Hadronic events are selected by a minimum of five charged tracks, total visible energy greater than 15% of the center-of-mass energy, and a charged track vertex consistent with the nominal interaction point. To reject continuum we require that the Fox-Wolfram moment R_2 be less than 0.3 [6].

Track candidates are required to pass through a common spatial point defined by origin of all tracks. Tracks with momentum below 900 MeV/c are required to have ionization loss in the drift chamber within 3σ of their assigned mass.¹ (These requirements are not imposed on slow charged pions from D^{*+} decay.) Photon candidates are required to be within the “good barrel region,” within 45° of the normal to the beam line, and have an energy distribution in the CsI calorimeter consistent with that of an electromagnetic shower. To select π^0 's, we require that the diphoton invariant mass be between -3.0 to $+2.5\sigma$, where σ varies with momentum and has an average value of approximately 5.5 MeV. For each two-photon mass combination σ is calculated. After candidate selection the two-photon's are kinematically fit by constraining their invariant mass to that of the

¹Here and throughout this paper σ indicates an r.m.s. error.

π^0 .

We select D^0 and D^+ candidates via the decay modes shown in Table 1. We require that the invariant mass of the D candidates lie within $\pm 2.5\sigma$ of the known D masses. The σ 's are also listed in Table 1. The D^0 widths vary with the D^0 momentum, p , (units of MeV).

We select D^{*+} candidates by imposing the addition requirement that the mass difference between π^+D^0 and D^0 combinations is within $\pm 2.5\sigma$ of the known mass difference. For the D^{*0} , we use the same requirement for the π^0D^0 decay. The mass difference resolutions are 0.63 and 0.90 MeV, for the π^+D^0 and π^0D^0 modes, respectively[7]

Table 1: Mass Resolutions (σ) in MeV

$D^+ \rightarrow K^- \pi^+ \pi^+$	$D^0 \rightarrow K^- \pi^+$	$D^0 \rightarrow K^- \pi^+ \pi^0$	$D^0 \rightarrow K^- \pi^+ \pi^+ \pi^-$
6.0	$p \times 0.93 \times 10^{-3} + 6.0$	$p \times 0.68 \times 10^{-3} + 11.6$	$p \times 0.92 \times 10^{-3} + 4.7$

3 Observation of $\bar{B}^0 \rightarrow D^{*+} \pi^+ \pi^- \pi^- \pi^0$ Decays

3.1 B Candidate Selection

We start by investigating the $D^{*+}(4\pi)^-$ final state.² The D^{*+} candidates are combined with all combinations of $\pi^+ \pi^- \pi^- \pi^0$ mesons.

Next, we calculate the difference between the beam energy, E_{beam} , and the measured energy of the five particles, ΔE . The ‘‘beam constrained’’ invariant mass of the B candidates, M_B , is computed from the formula

$$M_B^2 = E_{beam}^2 - \left(\sum_i \vec{p}_i \right)^2 . \quad (1)$$

To further reduce backgrounds we define

$$\chi_b^2 = \left(\frac{\Delta M_{D^*}}{\sigma(\Delta M_{D^*})} \right)^2 + \left(\frac{\Delta M_D}{\sigma(\Delta M_D)} \right)^2 + \sum_{n(\pi^0)} \left(\frac{\Delta M_{\pi^0}}{\sigma(\Delta M_{\pi^0})} \right)^2 , \quad (2)$$

where ΔM_{D^*} is the computed $D^* - D^0$ mass difference minus the nominal value, ΔM_D is the invariant candidate D^0 mass minus the known D^0 mass and ΔM_{π^0} is the measured $\gamma\gamma$ invariant mass minus the known π^0 mass. All π^0 's in the final state are included in the sum. The σ 's are the measurement errors. We select candidate events in each mode requiring that $\chi_b^2 < C_n$, where C_n varies for each decay D^0 decay mode. For the $Kn\pi$ decay modes we use $C_n = 12, 8,$ and $6,$ respectively.

3.2 Branching Fraction and $(4\pi)^-$ Mass Spectrum

We start with the $D^0 \rightarrow K^- \pi^+$ decay mode. We show the candidate B mass distribution, M_B , for ΔE in the side-bands from -5.0 to -3.0σ and 5.0 to 3.0σ on Fig. 1(a). The ΔE resolution is 18 MeV (σ). This gives a good representation of the background in the signal region. We fit this distribution with a shape given as

$$back(r) = p_1 r \sqrt{1 - r^2} e^{-p_2(1 - r^2)} , \quad (3)$$

where $r = M_B/5.2895$, and the p_i are parameters given by the fit.

²In this paper $(4\pi)^-$ will always denote the specific combination $\pi^+ \pi^- \pi^- \pi^0$.

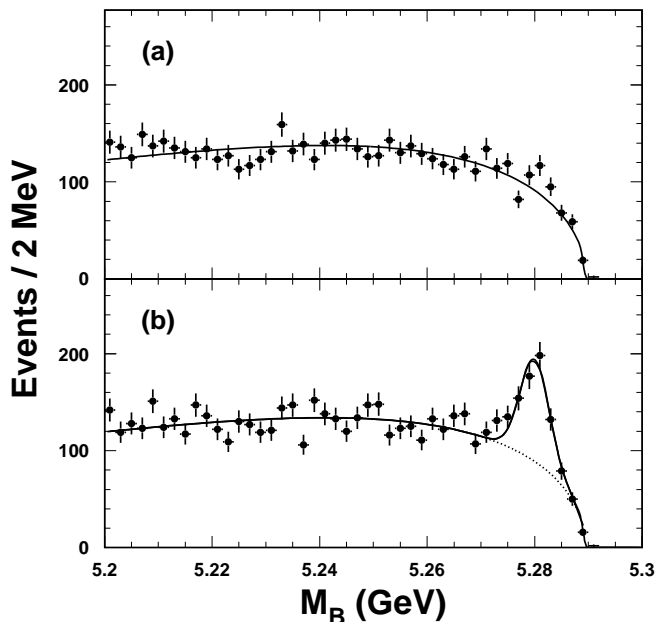


Figure 1: The B candidate mass spectra for the final state $D^{*+}\pi^+\pi^-\pi^-\pi^0$, with $D^0 \rightarrow K^-\pi^+$ (a) for ΔE sidebands and (b) for ΔE consistent with zero. The curve in (a) is a fit to the background distribution described in the text, while in (b) the shape from (a) is used with the normalization allowed to float and a signal Gaussian of width 2.7 MeV is added.

We next view the M_B distribution for events having ΔE within 2σ around zero in Fig. 1(b). This distribution is fit with a Gaussian signal function of width 2.7 MeV and the background function found above whose normalization is allowed to vary. We find 358 ± 29 events in the signal peak.

We repeat this procedure for the other two D^0 decay modes. The M_B spectrum for ΔE sidebands and signal region is shown in Fig. 2. The ΔE resolution is 22 MeV in the $K^-\pi^+\pi^0$ mode and 18 MeV in the $K^-\pi^+\pi^+\pi^-$ mode. Signal to background ratios are worse in these two modes, but the significance is still large. The number of signal events in each mode are shown in Table 2.

Table 2: Event numbers for the $D^{*+}\pi^+\pi^-\pi^-\pi^0$ final state

D^0 Decay Mode	Fitted # of events (%)
$K^-\pi^+$	358 ± 29
$K^-\pi^+\pi^0$	543 ± 49
$K^-\pi^+\pi^+\pi^-$	329 ± 41

We choose to determine the branching fraction using only the $D^0 \rightarrow K^-\pi^+$ decay mode because of the relatively large backgrounds in the other modes and the decreased systematic error due to having fewer particles in the final state. In order to find the branching ratio we use the Monte Carlo generated efficiency, shown in Fig. 3 as a function of $(4\pi)^-$ mass. The efficiency falls off at larger $(4\pi)^-$ masses because the detection of the slow π^+ from the D^{*+} decay becomes increasingly

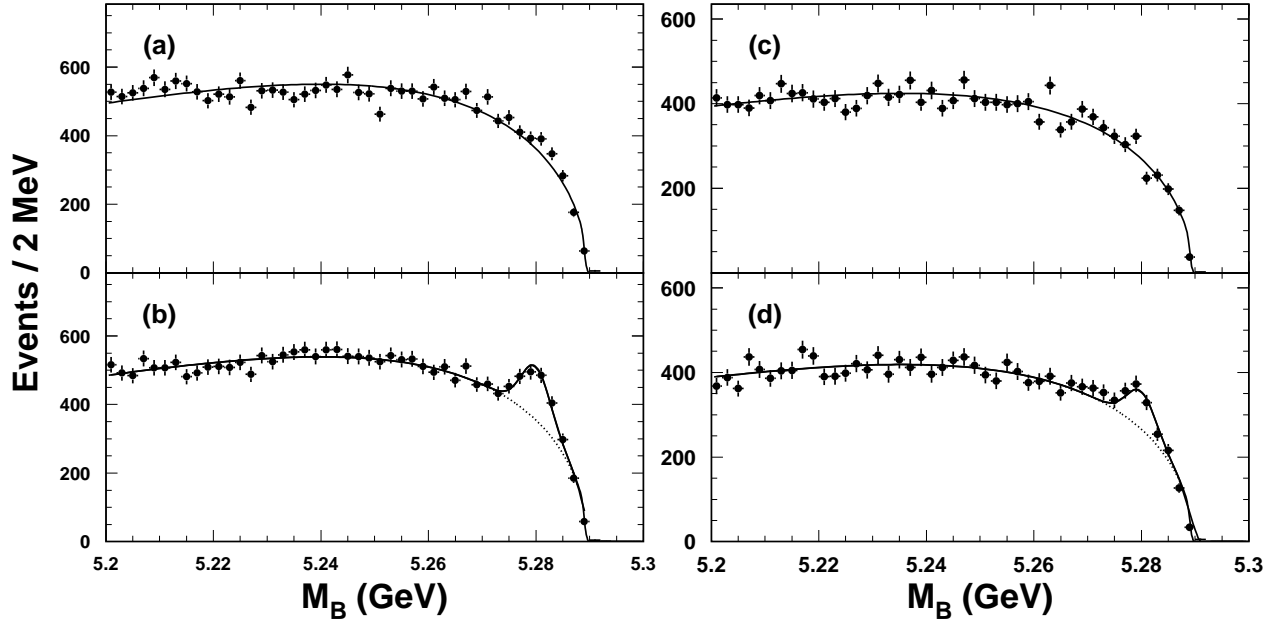


Figure 2: The B candidate mass spectra for the final state $D^{*+}\pi^+\pi^-\pi^-\pi^0$, the left-side plots are for $D^0 \rightarrow K^-\pi^+\pi^0$ (a) ΔE sidebands, (b) for ΔE consistent with zero; the right-side plots are for $D^0 \rightarrow K^-\pi^+\pi^+\pi^-$ (c) ΔE sidebands, (d) for ΔE consistent with zero. The curves in the top plots, (a) and (c), are fits to the background distribution described in the text, while in the bottom plots, (b) and (d), the shapes from (a) and (c) are used with the normalization allowed to float and a signal Gaussian of width 2.7 MeV is added.

difficult. Since the efficiency varies with mass we need to determine the $(4\pi)^-$ mass spectrum. To rid ourselves of the problem of the background shape, we fit the B candidate mass spectrum in 50 MeV bins of $(4\pi)^-$ mass. (The mass resolution is approximately 12 MeV.) The resulting $(4\pi)^-$ mass spectrum is shown in Fig. 4. There are indications of a low mass structure around 1.4 GeV. This will be investigated further in this paper.

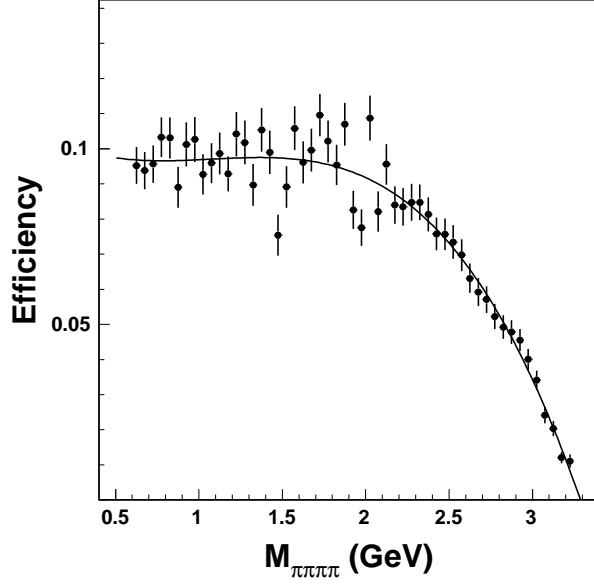


Figure 3: The efficiency for the final state $D^{*+}\pi^+\pi^-\pi^-\pi^0$, with $D^0 \rightarrow K^-\pi^+$.

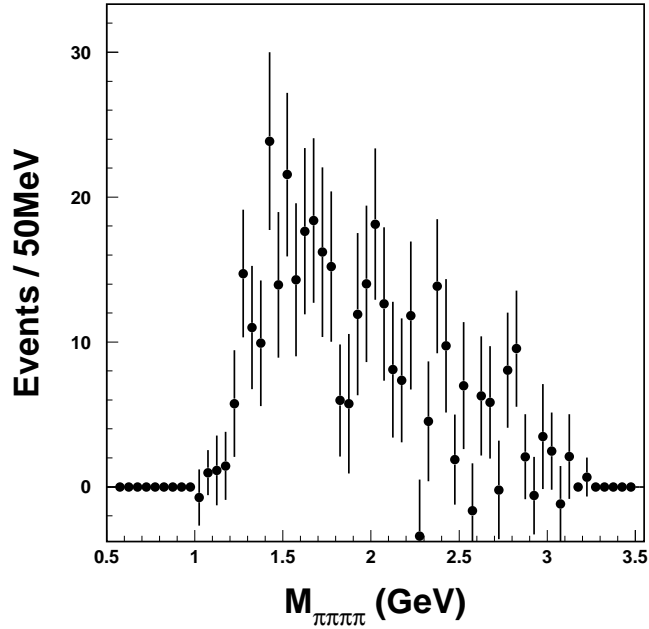


Figure 4: The invariant mass spectra of $\pi^+\pi^-\pi^-\pi^0$ for the final state $D^{*+}\pi^+\pi^-\pi^-\pi^0$, with $D^0 \rightarrow K^-\pi^+$, found by fitting the B yield in bins of 4π mass.

We find

$$\mathcal{B}(\bar{B}^0 \rightarrow D^{*+}\pi^+\pi^+\pi^-\pi^0) = (1.72 \pm 0.14 \pm 0.24)\% \quad . \quad (4)$$

The systematic error arises mainly from our lack of knowledge about the tracking and π^0 efficiencies. We assign errors of $\pm 2.2\%$ on the efficiency of each charged track, $\pm 5\%$ for the slow

pion from the D^{*+} , and $\pm 5.4\%$ for the π^0 . The error due to the background shape is evaluated in three ways. First of all, we change the background shape by varying the fitted parameters by 1σ . This results in a change of $\pm 3\%$. Secondly, we allow the shape, p_2 , to vary (the normalization, p_1 , was already allowed to vary). This results in 3.8% increase in the number of events. Finally, we choose a different background function

$$back'(r) = p_1 r \sqrt{1 - r^2} (1 + p_2 r + p_3 r^2 + p_4 r^3) \quad , \quad (5)$$

and repeat the fitting procedure. This results in a 3.7% decrease in the number of events. Taking a conservative estimate of the systematic error due to the background shape we arrive at $\pm 3.8\%$. We use the current particle data group values for the relevant D^{*+} and D^0 branching ratios of $(68.3 \pm 1.4)\%$ ($D^{*+} \rightarrow \pi^+ D^0$) and $(3.85 \pm 0.09)\%$ ($D^0 \rightarrow K^- \pi^+$), respectively [1]. The relative errors, 2.0% for the D^{*+} branching ratio and 2.3% for the D^0 are added in quadrature to the other sources of systematic error, yielding a total systematic error of 10% .

We wish to search for narrow structures. However, we cannot fit the B mass spectrum in small $(4\pi)^-$ mass intervals due to a lack of statistics. Thus we plot the $(4\pi)^-$ mass for events in the M_B peak for the $D^0 \rightarrow K^- \pi^+$ mode and the sum of all three modes in Fig. 5. We also plot two background samples: events at lower M_B (5.203 - 5.257 GeV) and those in the ΔE sideband separately. First we view the plots in the canonical 50 MeV bins. Both background distributions give a consistent if somewhat different estimates of the background shape. (Each background distribution has been normalized to the absolute number of background events as determined by the fit to the M_B distribution.) In any case no prominent narrow structures appear in the histograms for the 10 MeV binning.

4 The $\overline{B}^0 \rightarrow D^{*+} \omega \pi^-$ Reaction

To investigate the composition of the $(4\pi)^-$ final state, we now investigate the $\pi^+ \pi^- \pi^0$ mass spectrum for the events in the B peak. All three D^0 decay modes are used. We show the $\pi^+ \pi^- \pi^0$ invariant mass distribution for events in the B mass peak in Fig. 6 (there are two combinations per event). A clear signal is visible at the ω . The histograms on the figure are for events either in the lower M_B range, from 5.203 GeV to 5.257 GeV, or in the previously defined ΔE sidebands; no ω signal is visible.

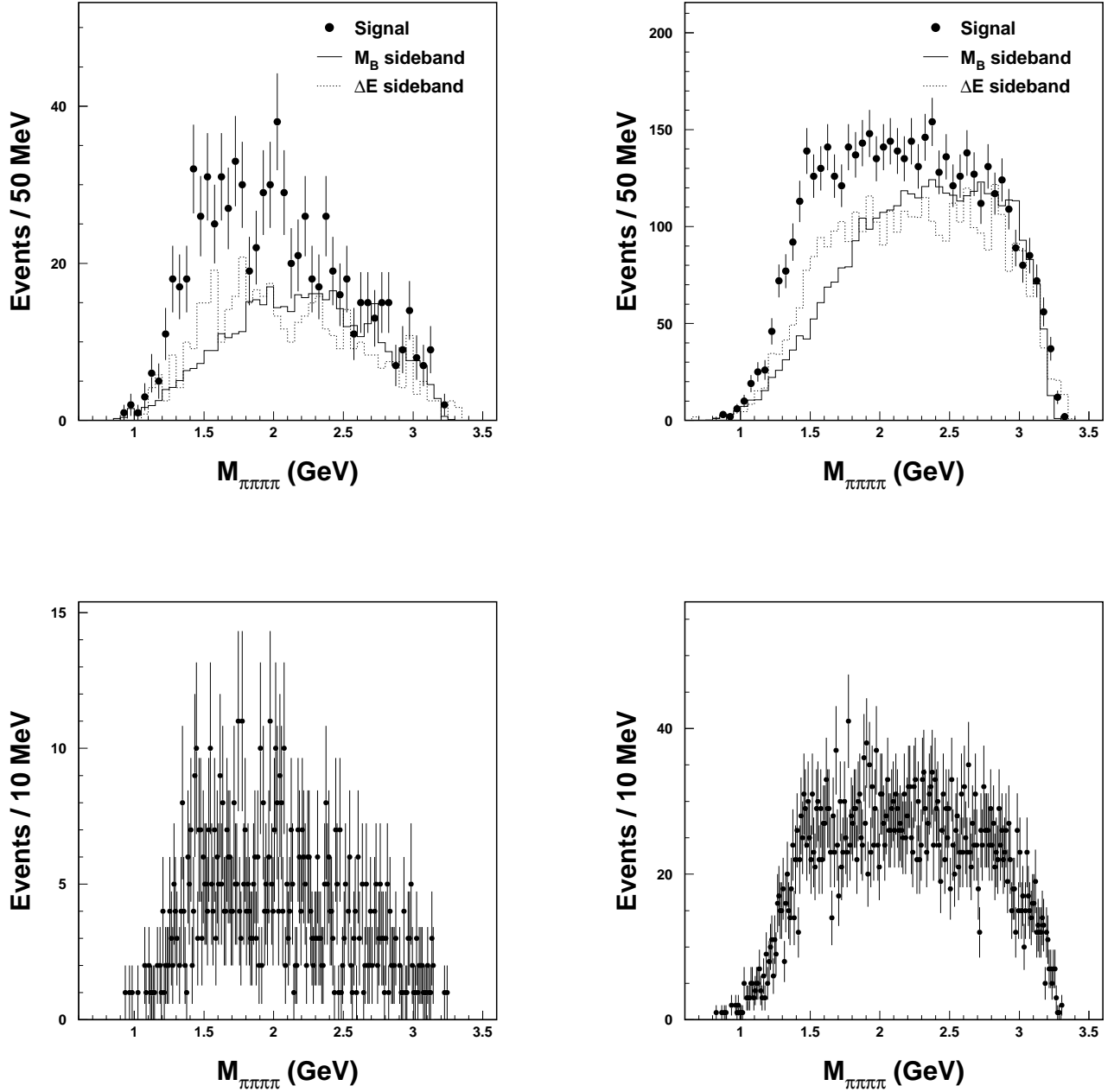


Figure 5: The invariant mass spectra of $\pi^+\pi^-\pi^-\pi^0$ for the final state $D^{*+}\pi^+\pi^-\pi^0$, with $D^0 \rightarrow K^-\pi^+$ (upper left), and the sum of all three D^0 decay modes (upper right). Events are selected by being within 2σ of the B mass. The solid histogram is the background estimate from the M_B lower sideband and the dashed histogram is from the ΔE sidebands; both are normalized to the fitted number of background events. The same distributions in smaller bins (lower plots).

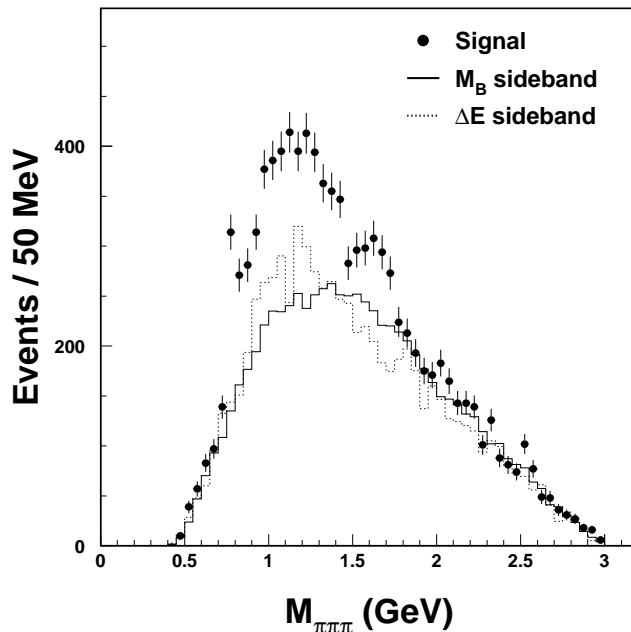


Figure 6: The invariant mass spectra of $\pi^+\pi^-\pi^0$ for the final state $D^{*+}\pi^+\pi^-\pi^-\pi^0$ for all three D^0 decay modes. The solid histogram is the background estimate from the M_B lower sideband and the dashed histogram is from the ΔE sidebands; both are normalized to the fitted number of background events.

The purity of the ω sample can be further improved by restricting candidates to certain regions of the Dalitz plot of the decay products. We define a cut on the Dalitz plot as follows. Let T_0 , T_+ and T_- be the kinetic energies of the pions, and Q be the difference between the ω mass, M_ω , and the mass of the 3 pions. We define two orthogonal coordinates X and Y , where

$$X = 3T_0/Q - 1 \quad (6)$$

$$Y = \sqrt{3}(T_+ - T_-)/Q \quad (7)$$

The kinematic limit that defines the Dalitz plot boundary is defined as

$$Y_{boundary}^2 = \frac{1}{3}(X_{boundary} + 1)(X_{boundary} + 1 + a)(1 + b/(X_{boundary} + 1 - c)) \quad (8)$$

where $a = 6m_0/Q$, $b = 6m^2/(M_\omega Q)$, $c = 3(M_\omega - m_0)^2/(2M_\omega Q)$, m is the mass of a charged pion and m_0 the mass of the neutral pion.

For any set of three pion kinetic energies, we define a variable r , properly scaled to the kinematic limit as

$$r = \sqrt{\frac{X^2 + Y^2}{X_{boundary}^2 + Y_{boundary}^2}} \quad (9)$$

where the boundary values are found by following the radial vector from (0,0) through (X, Y) .

For events in the B mass peak we show in Fig. 7 the $\pi^+\pi^-\pi^0$ invariant mass for three different cuts on r . The ω signal is purified by using a selection on r .

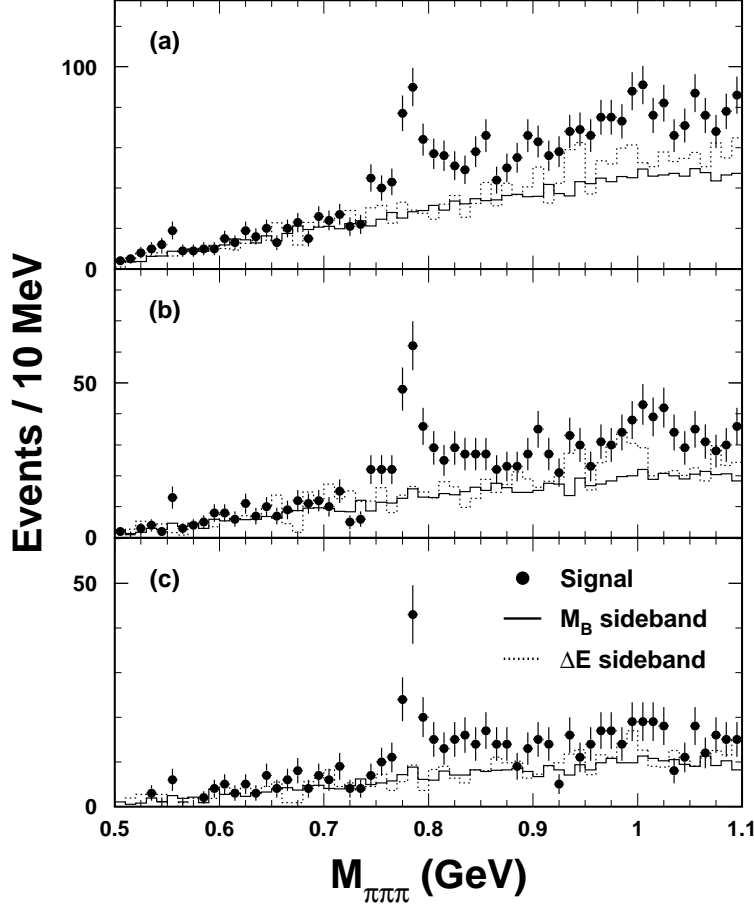


Figure 7: The invariant mass spectra of $\pi^+\pi^-\pi^0$ for the final state $D^{*+}\pi^+\pi^-\pi^0$ for all three D^0 decay modes for three selections on r : (a) 1, (b) 0.7 and (c) 0.5. The solid histogram is the background estimate from the M_B lower sideband and the dashed histogram is from the ΔE sidebands; both are normalized to the fitted number of background events.

For further analysis we select ω candidates within the $\pi^+\pi^-\pi^0$ mass window of 782 ± 20 MeV with $r < 0.7$. We also abandon the χ^2 cut as background is less of a problem. In Fig. 8 we show the B candidate mass distribution for the $D^{*+}\omega\pi^-$ final state summing over all three D^0 decay modes. (The signal is fit with the same prescription as before.) There are 136 ± 15 events in the peak.

In Fig. 9 we show the $\omega\pi^-$ mass spectrum in the left-side plot. The solid histogram shows events from the lower M_B sideband region suitably normalized. The dotted histogram shows the background estimate from the ΔE sidebands, again normalized. In the signal distribution there is a wide structure around 1.4 GeV, that is inconsistent with background. We re-determine the $\omega\pi^-$ mass distribution by fitting the M_B distribution in bins of $\omega\pi^-$ mass, and this is shown on the right-side. Fitting to a Breit-Wigner function, we find a peak value of 1416 ± 37 MeV and a width of 402 ± 47 MeV. These numbers change to 1432 ± 37 MeV and 376 ± 47 MeV, respectively, after applying a correction for the variation of efficiency with mass.

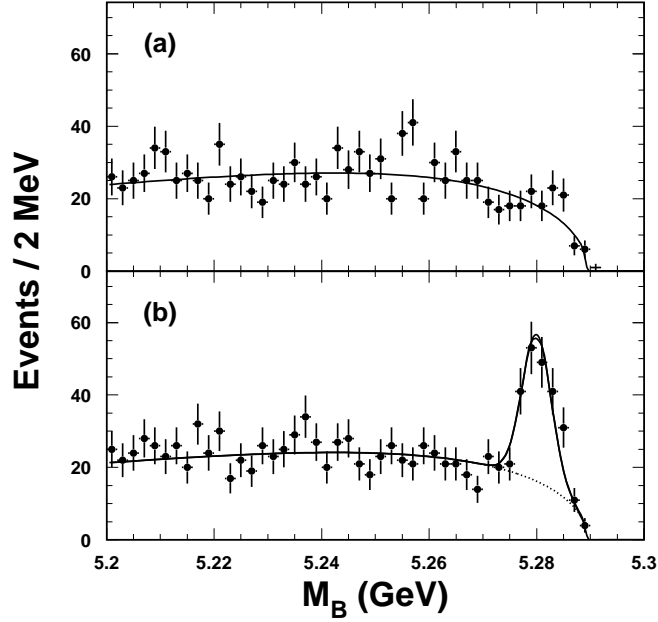


Figure 8: The M_B spectra for $D^{*+}\omega\pi^-$ for all three D^0 decay modes. (a) ΔE sidebands and (b) ΔE around zero.

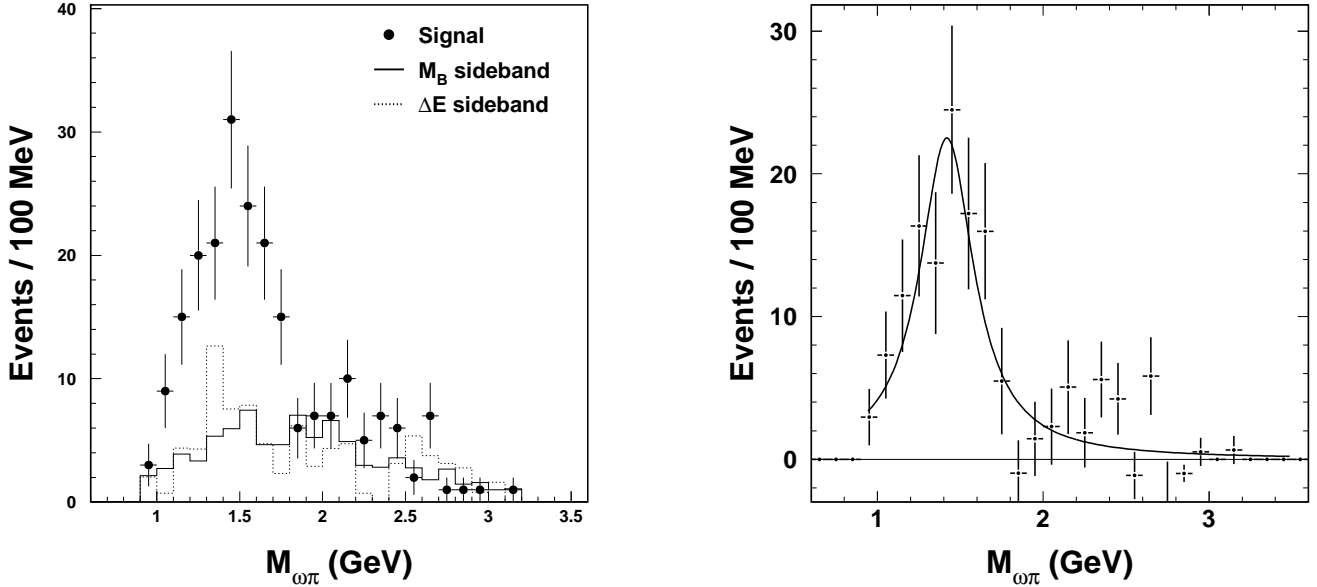


Figure 9: The invariant mass spectra of $\omega\pi^-$ for the final state $D^{*+}\pi^+\pi^-\pi^-\pi^0$ for all three D^0 decay modes. (left) The solid histogram is the background estimate from the M_B lower sideband and the dashed histogram is from the ΔE sidebands; both are normalized to the fitted number of background events. (right) The mass spectrum determined from fitting the M_B distribution and fit to a Breit-Wigner function.

Knowing the $\omega\pi^-$ mass dependence of the efficiency we evaluate the branching fraction:

$$\mathcal{B}(\overline{B}^0 \rightarrow D^{*+}\omega\pi^-) = (0.29 \pm 0.03 \pm 0.04)\% \quad . \quad (10)$$

We tentatively label the state at 1432 MeV the A^- and investigate its properties later. The $\omega\pi^-$ comprises about 17% of the $(4\pi)^-$ final state. All of the $\omega\pi^-$ final state is consistent with coming from A^- decay.

5 Observation of $B^- \rightarrow D^{*0}\pi^+\pi^-\pi^-\pi^0$

We proceed in the same manner as for the \overline{B}^0 reaction with the exception that we use the $D^{*0} \rightarrow \pi^0 D^0$ decay mode and restrict ourselves to the $D^0 \rightarrow K^-\pi^+$ decay mode only due to large backgrounds in the other modes. The χ^2 is calculated according to equation 2 and we use a cut value of 8. The M_B distributions for ΔE sidebands and signal data are shown in Fig. 10 for the $D^0 \rightarrow K^-\pi^+$ decay mode. We see a signal of 195 ± 26 events yielding a branching fraction of

$$\mathcal{B}(B^- \rightarrow D^{*0}\pi^+\pi^-\pi^-\pi^0) = (1.80 \pm 0.24 \pm 0.25)\% \quad . \quad (11)$$

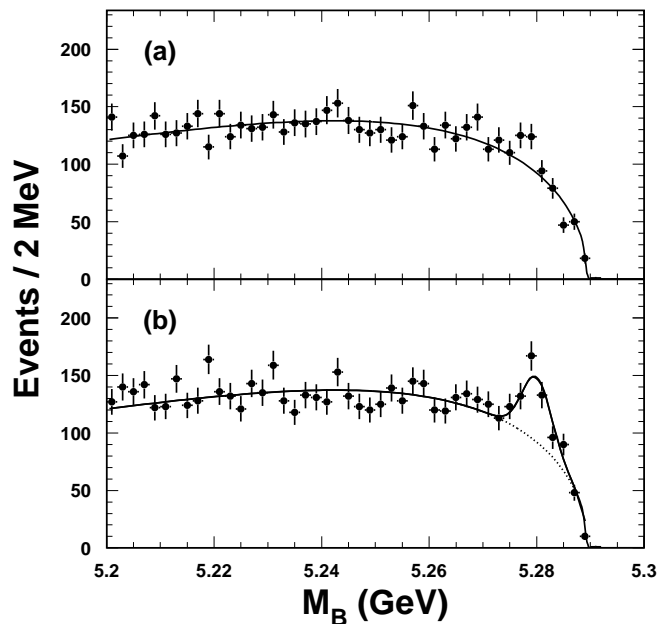


Figure 10: The B candidate mass spectra for the final state $D^{*0}\pi^+\pi^-\pi^-\pi^0$, with $D^0 \rightarrow K^-\pi^+$ (a) for ΔE sidebands and (b) for ΔE consistent with zero. The curve in (a) is a fit to the background distribution described in the text, while in (b) the shape from (a) is used with the normalization allowed to float and a signal Gaussian of width 2.7 MeV is added.

The $\pi^+\pi^-\pi^0$ mass spectrum shown in Fig. 11 shows the presence of an ω . Selecting on the presence of an ω with $r < 0.7$ we show the sideband and signal plots in Fig. 12. (Here we do not use the previously defined χ^2 cut.) The branching ratio is

$$\mathcal{B}(B^- \rightarrow D^{*0}\omega\pi^-) = (0.45 \pm 0.10 \pm 0.07)\% \quad . \quad (12)$$

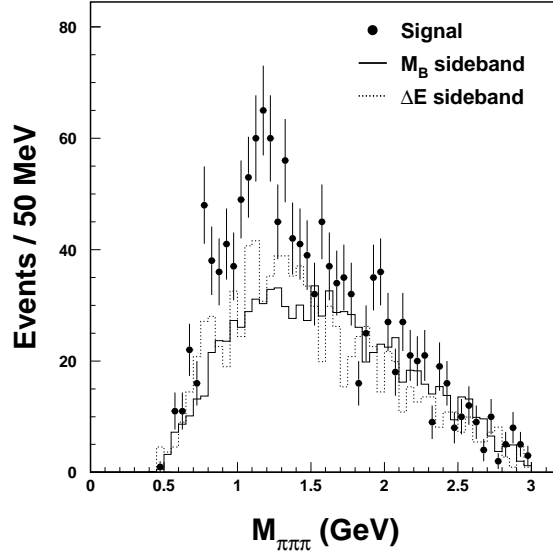


Figure 11: The invariant mass spectra of $\pi^+\pi^-\pi^0$ for the final state $D^{*0}\pi^+\pi^-\pi^-\pi^0$ for the $D^0 \rightarrow K^-\pi^+$ decay mode. The solid histogram is the background estimate from the M_B lower sideband and the dashed histogram is from the ΔE sidebands; both are normalized to the fitted number of background events. There are two combinations per event.

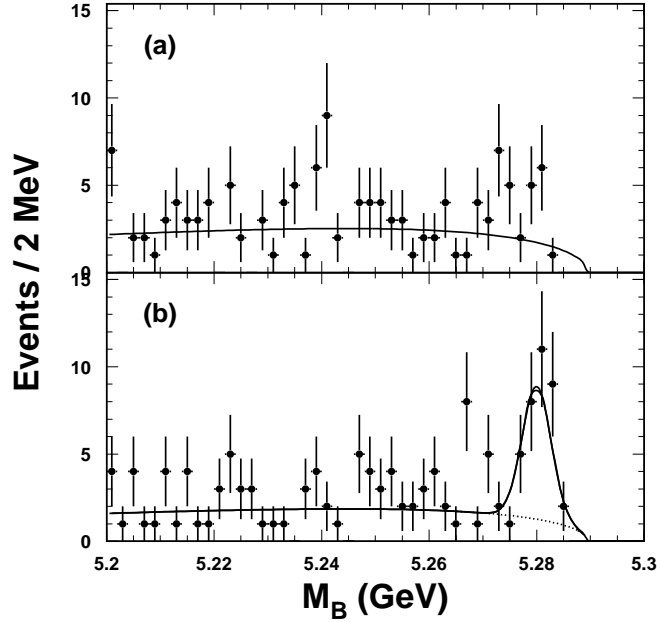


Figure 12: The M_B spectra for $D^{*0}\omega\pi^-$ for the $D^0 \rightarrow K^-\pi^+$ decay mode. (a) ΔE sidebands and (b) ΔE around zero.

In Fig. 13 we show the $\omega\pi^-$ mass spectrum. We see an enhancement at around 1.4 GeV as in the neutral B case. A fit to the data gives a mass of 1367 ± 75 MeV and width of 439 ± 135 MeV, consistent within the large errors with the \overline{B}^0 case. (We do not have enough statistics here to fit the M_B distribution in bins of $\omega\pi^-$ mass.) The $\omega\pi^-$ fraction of the $(4\pi)^-$ final state is 25%, and all the $\omega\pi^-$ is consistent with coming from the A^- .

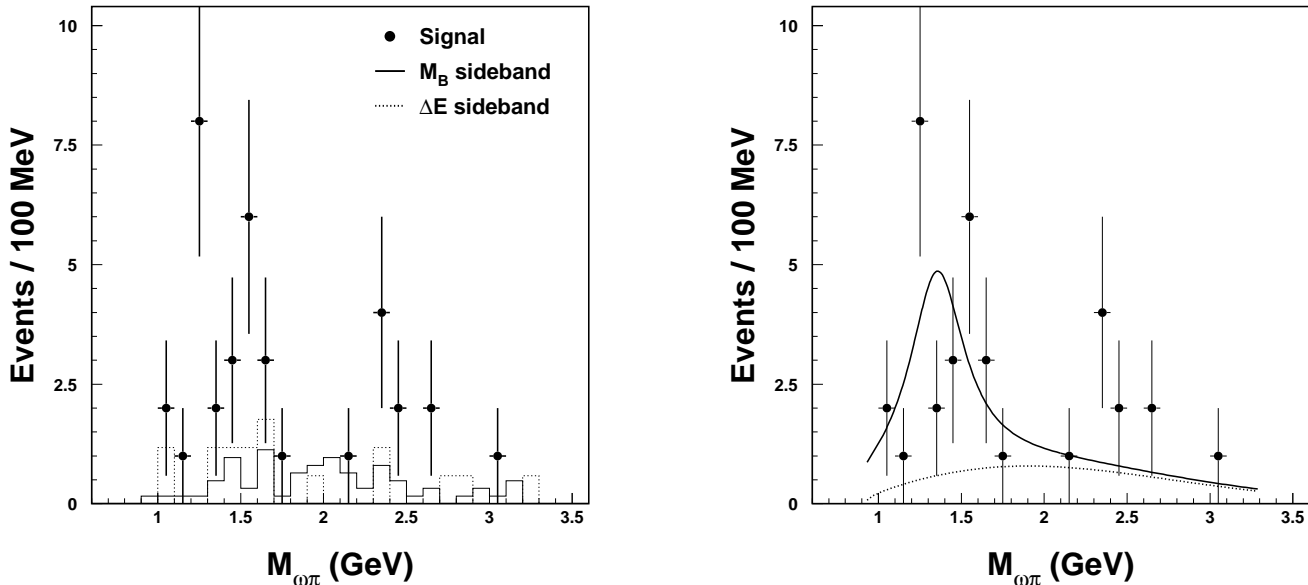


Figure 13: The invariant mass spectra of $\omega\pi^-$ for the final state $D^{*0}\pi^+\pi^-\pi^-\pi^0$ for the $D^0 \rightarrow K^-\pi^+$ decay mode. (left) The solid histogram is the background estimate from the M_B lower sideband and the dashed histogram is from the ΔE sidebands; both are normalized to the fitted number of background events. (right) The data fit to a Breit-Wigner signal and a smooth background function.

6 Analysis of $D^{*+}\omega\pi^-$ Decay Angular Distributions

The A^- is produced along with a spin-1 D^* from a spin-0 B . If the A^- is spin-0 the D^* would be fully polarized in the $(J, J_z) = (1, 0)$ state. If the A^- were to be spin-1 any combinations of z-components would be allowed. It is natural then to examine the helicity angle of the D^{*+} by viewing the cosine of the helicity angle of the π^+ with respect to the B in the D^{*+} rest frame.

Another decay angle that can be examined is that of the $\omega\pi$ system. If the A^- is spin-0, the ω is polarized in the $(1, 0)$ state and may be if the A^- is spin-1. Here the helicity angle is defined as the angle between the normal to the ω decay plane and the direction of the A^- in the ω rest frame. For a spin-0 A^- the distribution will be cosine-squared. Again full polarization is possible if the A^- is other than spin-0, but any distribution other than cosine-squared would demonstrate that the spin is not equal to zero.

For this analysis we use all three D^0 final states for the D^{*+} final state. To find the distributions we fit the number of events in the M_B candidate plot selected on different angle bins. The $\omega\pi$ mass is required to be between 1.1 and 1.9 GeV. This leaves 111 ± 13 events.

In Fig. 14 we show the helicity angle distribution, $\cos\theta_{D^*}$ for the D^* decay. The data have been corrected for acceptance. We also show the expectation for spin-0 from the Monte Carlo. The data have been fit for the fraction of longitudinal polarization. We find

$$\frac{\Gamma_L}{\Gamma} = 0.63 \pm 0.09 . \quad (13)$$

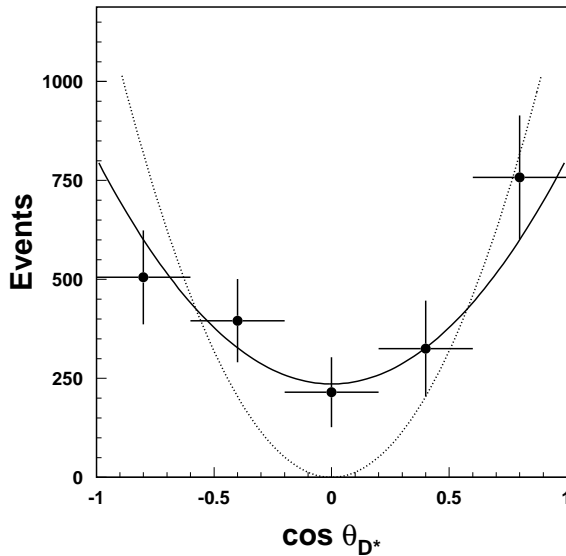


Figure 14: The cosine of the angle between the D^0 and the D^* flight direction in the D^* rest frame for the D^*A^- final state (solid points) along with a fit (solid curve) allowing the amount of longitudinal and traverse polarization to vary. The dotted curve is the expectation for a spin-0 A^- .

The $\cos\theta_{D^*}$ distribution is not consistent with full polarization, yielding a χ^2 of 17.7 for 5 degrees of freedom. The helicity angle distribution for the $A^- \rightarrow \omega\pi^-$, $\cos\theta_\omega$, is shown on Fig. 15. Furthermore the $\cos\theta_\omega$ distribution is quite inconsistent with a $\cos^2\theta_\omega$, yielding a χ^2 of 109 for 5 degrees of freedom. Therefore, we rule out a spin-0 assignment for the A^- .

To determine the J^P we need a more well defined final state. This is provided by analysis of $B \rightarrow D\omega\pi^-$ decays.

7 Observation of $\bar{B} \rightarrow D\omega\pi^-$ Decays

7.1 B candidate selection

Here we study the reactions $\bar{B} \rightarrow D\omega\pi^-$, with either a $D^0 \rightarrow K^-\pi^+$ or $D^+ \rightarrow K^-\pi^+\pi^+$ decay. Other D^0 or D^+ decays have substantially larger backgrounds.

Although we are restricting our search to ω 's, we define two $\pi^+\pi^-\pi^0$ samples. One within 20 MeV of the known ω mass (782 MeV) and the other in either low mass or high mass sideband defined as three π mass either between 732 and 752 MeV or between 812 and 832 MeV. We also require a cut on the ω Dalitz plot of $r < 0.7$.

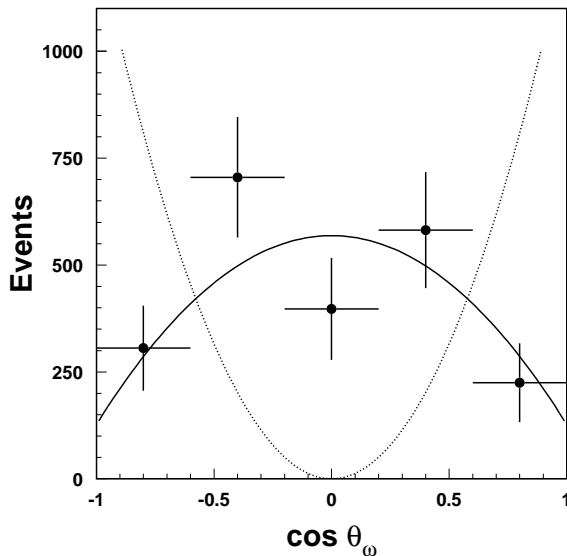


Figure 15: The cosine of the angle between the normal to the $\pi^+\pi^-\pi^0$ decay plane and the ω boost direction for the D^*A^- final state (solid points) along with a fit (solid curve) allowing the amount of longitudinal and transverse polarization to vary. The dotted curve is the expectation for a spin-0 A^- .

To reduce backgrounds we define

$$\chi_b^2 = \left(\frac{\Delta M_D}{\sigma(\Delta M_D)} \right)^2 + \left(\frac{\Delta M_\omega}{\sigma(\Delta M_\omega)} \right)^2 + \left(\frac{\Delta M_{\pi^0}}{\sigma(\Delta M_{\pi^0})} \right)^2, \quad (14)$$

where ΔM_D is the invariant candidate D^0 mass minus the known D^0 mass, ΔM_ω is the invariant candidate ω mass minus the known ω mass, and ΔM_{π^0} is the measured $\gamma\gamma$ invariant mass minus the known π^0 mass. The σ 's are the measurement errors. We select candidate events requiring that χ_b^2 is < 12 for the $K\pi$ mode and < 6 for the $K\pi\pi$.

7.2 $B^- \rightarrow D^0\omega\pi^-$ Signal

We start with the $D^0 \rightarrow K^-\pi^+$ decay mode, for events in the ω peak. We show the candidate B mass distribution, M_B , for ΔE in the side-bands from -7.0 to -3.0σ and 7.0 to 3.0σ on Fig. 16(a). The ΔE resolution is 18 MeV (σ). This gives a good representation of the background in the signal region. We fit this distribution with a shape given as

$$back(r) = p_1 r \sqrt{1 - r^2} e^{-p_2(1-r^2)}, \quad (15)$$

where $r = M_B/5.2895$, and the p_i are parameters given by the fit.

We next view the M_B distribution for events having ΔE within 2σ around zero in Fig. 16(b). This distribution is fit with a Gaussian signal function of width 2.7 MeV and the background function found above whose normalization is allowed to vary. We find 88 ± 14 events in the signal peak.

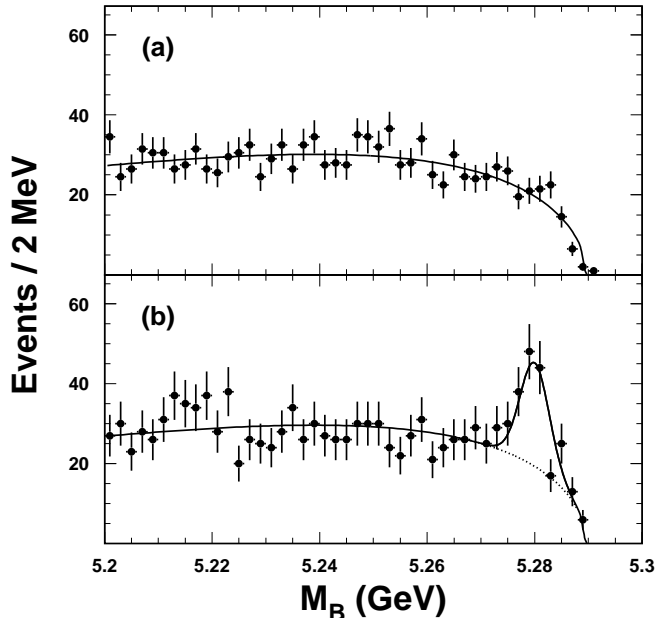


Figure 16: The B candidate mass spectra for the final state $D^0\omega\pi^-$, with $D^0 \rightarrow K^-\pi^+$. (a) for ΔE sidebands, and (b) for ΔE consistent with zero. The vertical scale in (a) was multiplied by 0.5 to facilitate comparison. The curve in (a) is a fit to the background distribution described in the text, while in (b) the shape from (a) is used with the normalization allowed to float and a signal Gaussian of width 2.7 MeV is added.

We repeat this procedure for events in the ω sidebands. We use for our χ_b^2 definition pseudo- ω masses in the sideband intervals. We show the M_B distribution for events in the ΔE sideband, defined above, and those having ΔE within 2σ around zero in Fig. 17. We find no significant signal.

7.3 $\bar{B}^0 \rightarrow D^+\omega\pi^-$ Signal

The same procedure followed for the D^0 final state is used for the D^+ final state. We show the candidate B mass distribution, M_B , for events in the ΔE side-band on Fig. 18(a). The ΔE resolution is 18 MeV (σ). This gives a good representation of the background in the signal region. We fit this distribution with a shape given in equation 15.

We next view the M_B distribution for events having ΔE within 2σ around zero in Fig. 18(b). This distribution is fit with a Gaussian signal function of width 2.7 MeV and the background function found above whose normalization is allowed to vary. We find 91 ± 18 events in the signal peak.

We repeat this procedure for events in the ω sidebands. We show the M_B distribution for both ΔE sidebands and ΔE within 2σ around zero in Fig. 19.

There is no evidence of any signal in the ω sideband plot, leading to the conclusion that the signal is associated purely with ω .

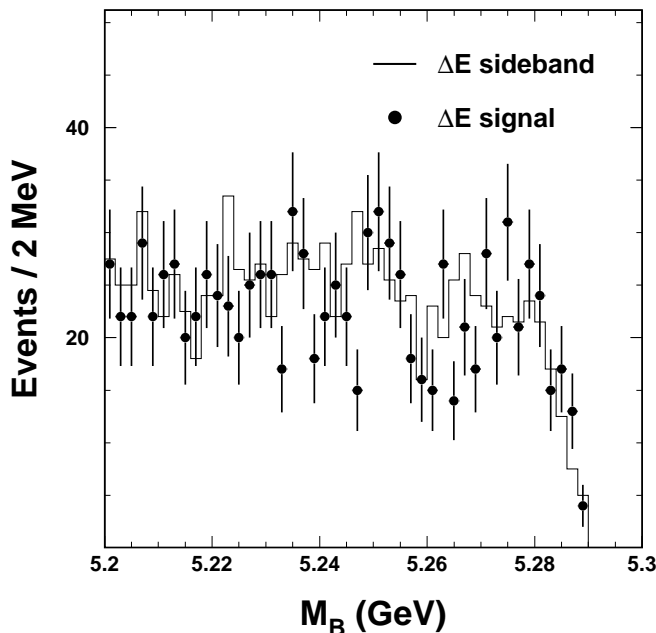


Figure 17: The B candidate mass spectra for the final state $D^0\omega\pi^-$, with $D^0 \rightarrow K^-\pi^+$ and ω sidebands (a) for ΔE sidebands and (b) for ΔE consistent with zero.

7.4 Branching Fractions

We determine the branching ratios, shown in Table 3, by performing a Monte Carlo simulation of the efficiencies in the two modes. We use the current particle data group values for the relevant ω , D^+ and D^0 branching ratios of $(88.8\pm 0.7)\%$ ($\omega \rightarrow \pi^+\pi^-\pi^0$), $(9.0\pm 0.6)\%$ ($D^+ \rightarrow K^-\pi^+\pi^+$) and $(3.85\pm 0.09)\%$ ($D^0 \rightarrow K^-\pi^+$) [1]. The efficiencies listed in the table do not include these branching ratios [8].

Table 3: Branching Fractions for the $D\omega\pi^-$ final state

D^0 Decay Mode	Fitted # of events	Efficiency	Branching Fraction (%)
$K^-\pi^+$	88 ± 14	0.064	$0.41\pm 0.07\pm 0.04$
$K^-\pi^+\pi^+$	91 ± 18	0.046	$0.28\pm 0.05\pm 0.03$

The systematic error arises mainly from our lack of knowledge about the tracking and π^0 efficiencies. We assign errors of $\pm 2.2\%$ on the efficiency of each charged track, and $\pm 5.4\%$ for the π^0 . The error due to the background shape is evaluated in three ways. First of all, we change the background shape by varying the fitted parameters by 1σ . This results in a change of $\pm 5.0\%$. Secondly, we allow the shape, p_2 , to vary (the normalization, p_1 , was already allowed to vary). This results in 5.5% increase in the number of events. Finally, we choose a different background function

$$back'(r) = p_1 r \sqrt{1-r^2} \left(1 + p_2 r + p_3 r^2 + p_4 r^3 \right) \quad , \quad (16)$$

and repeat the fitting procedure. This results in a 1.0% decrease in the number of events. Taking a conservative estimate of the systematic error due to the background shape we arrive at $\pm 5.5\%$.

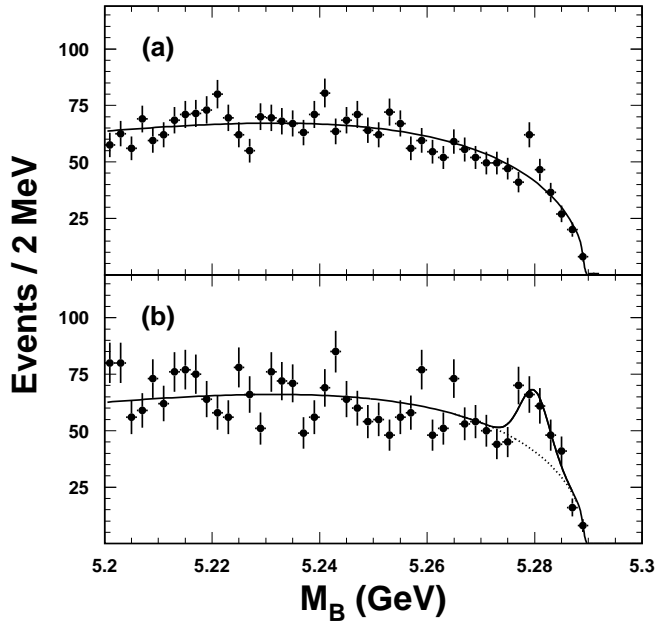


Figure 18: The B candidate mass spectra for the final state $D^+\omega\pi^-$, with $D^+ \rightarrow K^-\pi^+\pi^+$ (a) for ΔE sidebands and (b) for ΔE consistent with zero. The vertical scale in (a) was multiplied by 0.5 to facilitate comparison. The curve in (a) is a fit to the background distribution described in the text, while in (b) the shape from (a) is used with the normalization allowed to float and a signal Gaussian of width 2.7 MeV is added.

7.5 The $\omega\pi^-$ System

For all subsequent discussions we add the D^0 and D^+ final states together. We select sample of ω 's in the $\pi^+\pi^-\pi^0$ mass window of 782 ± 20 MeV using only combinations having $r < 0.7$ in the Dalitz plot.

In Fig. 20 we show the $\omega\pi^-$ mass spectrum in the left-side plot. The solid histogram shows events from the lower M_B sideband region (5.203 - 5.257 GeV) suitably normalized. The dotted histogram shows the background estimate from the ΔE sidebands, again normalized. In the signal distribution there is a wide structure around 1.4 GeV, that is inconsistent with background. We re-determine the $\omega\pi^-$ mass distribution by fitting the M_B distribution in bins of $\omega\pi^-$ mass, and this is shown on the right-side. Fitting to a Breit-Wigner function, we find a peak value of 1415 ± 43 MeV and a width of 419 ± 110 MeV. It should be kept in mind that this particular signal shape is assumed to be correct. Other resonant or non-resonant contributions could affect the mass and width.

This structure appears identical to the one we observed in $\bar{B} \rightarrow D^*\omega\pi^-$ decays.

7.6 Angular Distributions in $D\omega\pi^-$

We can determine the spin and parity of the A^- particle by studying the angular distributions characterizing its decay products. The decay chain that we are considering is $B \rightarrow A D$; $A \rightarrow \omega\pi$ and $\omega \rightarrow \pi^+\pi^-\pi^0$. The helicity formalism [9] is generally used in the analysis of these sequential

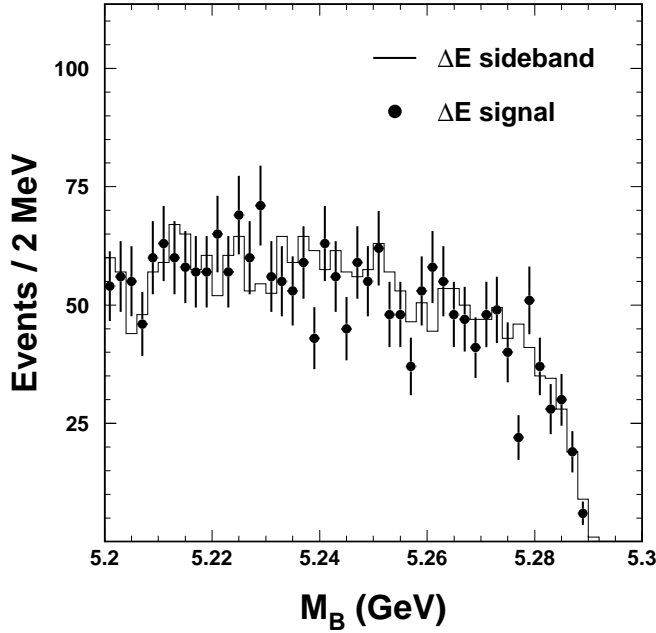


Figure 19: The B candidate mass spectra for the final state $D^+\omega\pi^-$, with $D^+ \rightarrow K^-\pi^+\pi^+$ and ω sidebands (a) for ΔE sidebands and (b) for ΔE consistent with zero.

decays. This formalism is well suited to relativistic problems involving particles with spin \vec{S} and momentum \vec{p} because the helicity operator $h = \vec{S} \cdot \vec{p}$ is invariant under both rotations and boosts along \hat{p} .

There are two relevant reference frames. The first one, that we will define $x_A y_A z_A$ is the rest frame of the A particle, with the z_A axis pointing in the A direction of motion in the B rest frame. The second one, $x_\omega y_\omega z_\omega$, is related to $x_A y_A z_A$ by the rotation through 3 Euler angles $\phi_A, \theta_A, -\phi_A$, as shown in Fig. 21. The angle ϕ_A defines the orientation of the plane containing the ω direction in the A rest frame and the z_A axis with respect to the $x_A - z_A$ plane. The x_A direction is arbitrary. The angles θ_ω and ϕ_ω define the orientation of the ω decay plane in the ω rest frame. Note that the A decay plane has an azimuthal angle ϕ_A both in the $x_A y_A z_A$ and in the $x_\omega y_\omega z_\omega$ references. As the angle ϕ_A is arbitrary, the only angle that has a physical meaning is $\chi = \phi_A - \phi_\omega$, the opening angle between the A decay plane and the ω decay plane.

Both the B meson and the D meson are pseudoscalar, therefore their helicity is 0. Thus A will be longitudinally polarized independently of its spin. In order to calculate the decay amplitude for this process, we need to sum over the ω helicity states:

$$A = \sum_{\lambda_\omega} D_{0\lambda_\omega}^{*J_A}(\phi_A, \theta_A, -\phi_A) D_{\lambda_\omega 0}^{*1}(\phi_\omega, \theta_\omega, -\phi_\omega) B_{\lambda_\omega 0}, \quad (17)$$

here $D_{\lambda_\omega}^{*1}(\phi_A, \theta_A, -\phi_A)$ is the rotation matrix that relates the $x_A y_A z_A$ and the $x_\omega y_\omega z_\omega$ frames and $D_{\lambda_\omega}^{*1}(\phi_\omega, \theta_\omega, -\phi_\omega)$ is the rotation matrix relating the $x_\omega y_\omega z_\omega$ and the direction of the normal to the ω decay plane $\hat{n}(\theta_\omega, \phi_\omega)$.

In general, there are three helicity amplitudes that contribute to this decay: B_{10} and B_{-10} , corresponding to a transverse ω polarization, and B_{00} , corresponding to a longitudinal ω polarization. This expression can be simplified by observing that $A \rightarrow \omega\pi$ is a strong decay and thus conserves

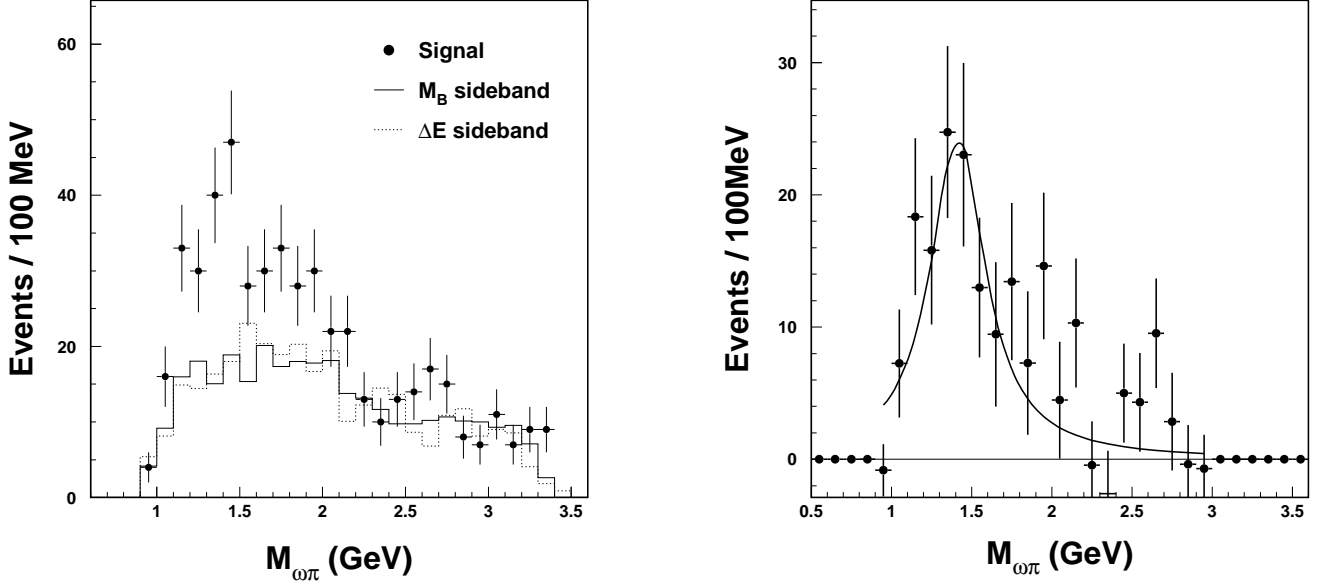


Figure 20: The invariant mass spectra of $\omega\pi^-$ for the final state $D\omega\pi^-$ for both D decay modes. (left) The solid histogram is the background estimate from the M_B lower sideband and the dashed histogram is from the ΔE sidebands; both are normalized to the fitted number of background events. (right) The mass spectrum determined from fitting the M_B distribution and fit to a Breit-Wigner function.

parity. Thus, the helicity amplitudes are related by the equation:

$$B_{10} = (-1)^{1-S(A)} \eta_A \eta_\omega \eta_\pi B_{-10}, \quad (18)$$

$$B_{00} = (-1)^{1-S(A)} \eta_A \eta_\omega \eta_\pi B_{00}. \quad (19)$$

where $S(A)$ is the spin of particle A and η_A, η_ω and η_π represent the intrinsic parity of the decaying particle and its decay products, respectively.

Eq. 18 relates the two transverse helicity amplitudes, while Eq. 19 forbids the presence of a longitudinal component under certain conditions. For example, if A is a 1^- object, ω has transverse polarization and $B_{-10} = -B_{10}$. When the sign in Eqs. 18-19 is positive, two parameters determined by the hadronic matrix element affect the angular distribution and thus we cannot fully determine it only on the basis of our assumptions on the A spin parity. We have carried out the calculation of the predicted angular distributions including spin assignment for A up to 2. The predicted angular distributions are summarized in Table 4.

The statistical accuracy of our data sample is not sufficient to do a simultaneous fit of the joint angular distributions shown above. Thus only the projections along the θ_A, θ_ω and χ are fitted, integrating out the remaining degrees of freedom. Table 5, gives the analytical form for these projections.

We determine the projections of these angular distributions by fitting the M_B distribution as a function of the various angular quantities $\cos\theta_A, \cos\theta_\omega, \chi$. We restrict the $\omega\pi^-$ mass range to be between 1.1 and 1.7 GeV, containing 104 events. In order to fit the angular distribution with theoretical expectations, we must correct the data for acceptances. We determine the

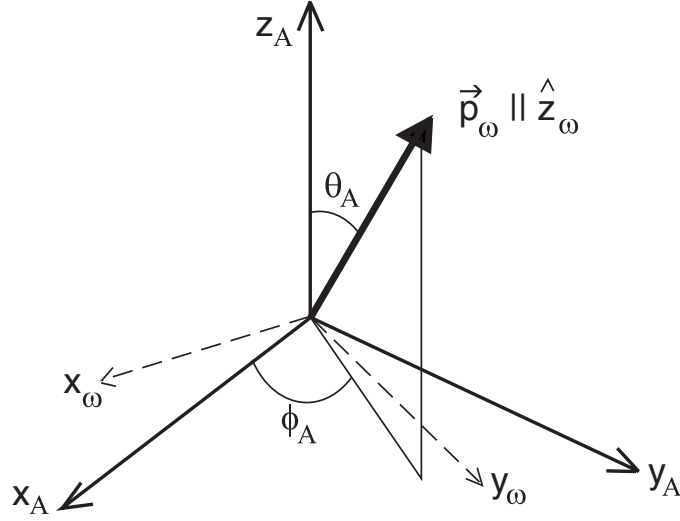


Figure 21: Relationship between the A rest frame $x_A y_A z_A$ and the ω rest frame $x_\omega y_\omega z_\omega$. x_A and x_ω lie in the same plane.

Table 4: Differential angular distributions (modulo a proportionality constant) predicted for different spin assignments.

J^n	$d\sigma/d \cos \theta_A d \cos \theta_\omega d\chi$
0^-	$ B_{00} ^2 \cos^2 \theta_\omega$
1^-	$ B_{10} ^2 \sin^2 \theta_A \sin^2 \theta_\omega \sin^2 \chi$
1^+	$ B_{10} ^2 \sin^2 \theta_A \sin^2 \theta_\omega^2 \cos^2 \chi + B_{00} ^2 \cos^2 \theta_A \cos^2 \theta_\omega$ $- 1/2 \text{Re}(B_{10} B_{00}^*) \sin 2\theta_A \sin 2\theta_\omega \cos \chi$
2^-	$3 B_{10} ^2 \sin^2 2\theta_A \sin^2 \theta_\omega \cos^2 \chi + B_{00} ^2 (3 \cos^2 \theta_A - 1)^2 \cos^2 \theta_\omega$ $-\sqrt{3} \text{Re}(B_{10} B_{00}^*) \sin 2\theta_A (3 \cos^2 \theta_A - 1) \sin 2\theta_\omega \cos \chi$
2^+	$3/4 B_{10} ^2 \sin^2 2\theta_A \sin^2 \theta_\omega \sin^2 \chi$

Table 5: Projection of the angular distributions along the $\cos \theta_A$, $\cos \theta_\omega$ and χ axes.

J^n	$d\sigma/d \cos \theta_A$	$d\sigma/d \cos \theta_\omega$	$d\sigma/d \chi$
0^-	$\frac{4\pi}{3} B_{00} ^2$	$4\pi B_{00} ^2 \cos^2 \theta_\omega$	$4/3 B_{00} ^2$
1^-	$\frac{4\pi}{3} B_{10} ^2 \sin^2 \theta_A$	$\frac{4\pi}{3} B_{10} ^2 \sin^2 \theta_\omega$	$\frac{8}{9} B_{10} ^2 \sin^2 \chi$
1^+	$\frac{4\pi}{3} (B_{10} ^2 \sin^2 \theta_A + B_{00} ^2 \cos^2 \theta_A)$	$\frac{4\pi}{3} (B_{10} ^2 \sin^2 \theta_\omega + B_{00} ^2 \cos^2 \theta_\omega)$	$\frac{4}{9} (4 B_{10} ^2 \cos^2 \chi + B_{00} ^2)$
2^-	$\frac{4\pi}{3} (3 B_{10} ^2 \sin^2 2\theta_A + B_{00} ^2 (3 \cos^2 \theta_A - 1)^2)$	$\frac{16\pi}{5} (B_{10} ^2 \sin^2 \theta_\omega + B_{00} ^2 \cos^2 \theta_\omega)$	$4 B_{10} ^2 \cos^2 \chi + B_{00} ^2$
2^+	$\pi B_{10} ^2 \sin^2 2\theta_A$	$\frac{4\pi}{5} B_{10} ^2 \sin^2 \theta_\omega$	$\frac{16}{15} B_{10} ^2 \sin^2 \chi$

acceptance correction by comparing the Monte Carlo generated angular distributions with the reconstructed distributions. The angular dependent efficiencies are shown in Fig. 22.

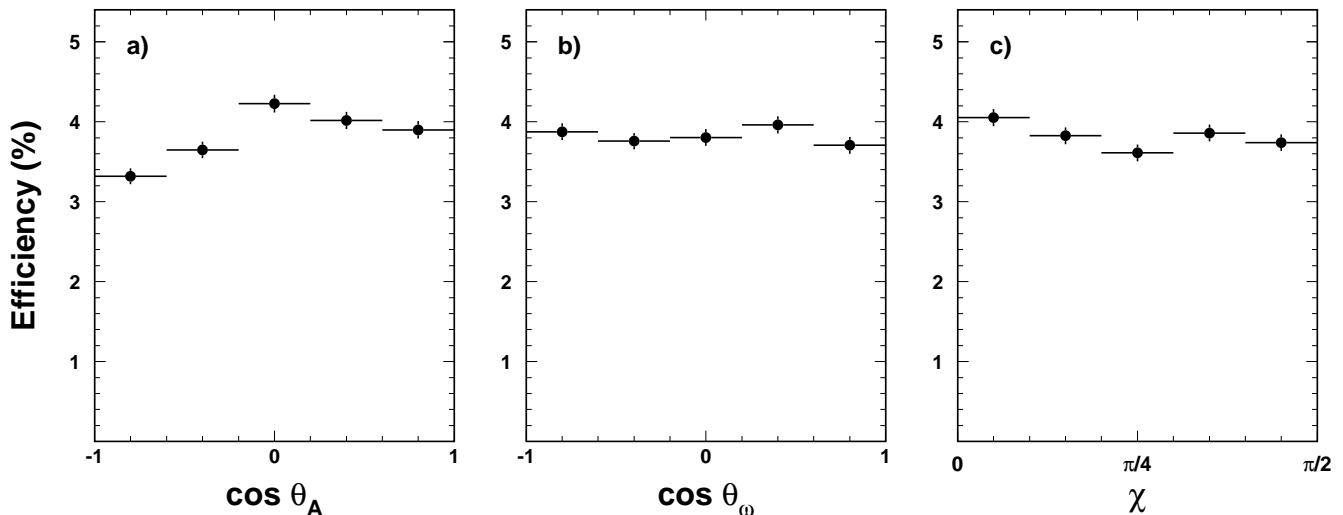


Figure 22: Reconstruction efficiency dependence on (a) $\cos \theta_A$, (b) $\cos \theta_\omega$, and (c) χ .

The corrected angular distributions are shown in Fig. 23. The data are fit to the expectations for the various J^P assignments. For the 0^- , 1^- and 2^+ assignments, the curves have a fixed shape. For the 1^+ and 2^- assignments we let the ratio between the longitudinal and transverse amplitudes vary to best fit the data. We notice that the ω polarization is very clearly transverse ($\sin^2 \theta_\omega$) and that infers a 1^- or 2^+ assignment.

We list in Table 6 the χ^2/dof for the different J^P assignments. The 1^- assignment is preferred, having a χ^2/dof of 1.7. The other assignments are clearly ruled out. The probability that we have a correct solution and χ^2/dof is 1.7 or greater is 3.8% [10].

Table 6: The χ^2 of angular fits

	0^-	1^+	1^-	2^+	2^-
χ^2/dof	7.0	4.5	1.7	3.2	5.3
probability	1.9×10^{-15}	3.3×10^{-8}	3.8%	2.7×10^{-5}	3.3×10^{-10}

8 Discussion of Nature of the A^-

We have found a 1^- object decaying into $\omega\pi^-$. A simple Breit-Wigner fit assuming a single resonance and no background gives a mass of 1418 ± 26 MeV with an intrinsic width of 382 ± 41 MeV. (The individual measurements are listed in Table 7). We have evaluated the systematic errors due to changes in the parameterization of the background shape in when fitting the M_B distributions in bins of $\omega\pi^-$ mass. This leads to an error in the mass of 19 MeV and 32 MeV in the width.

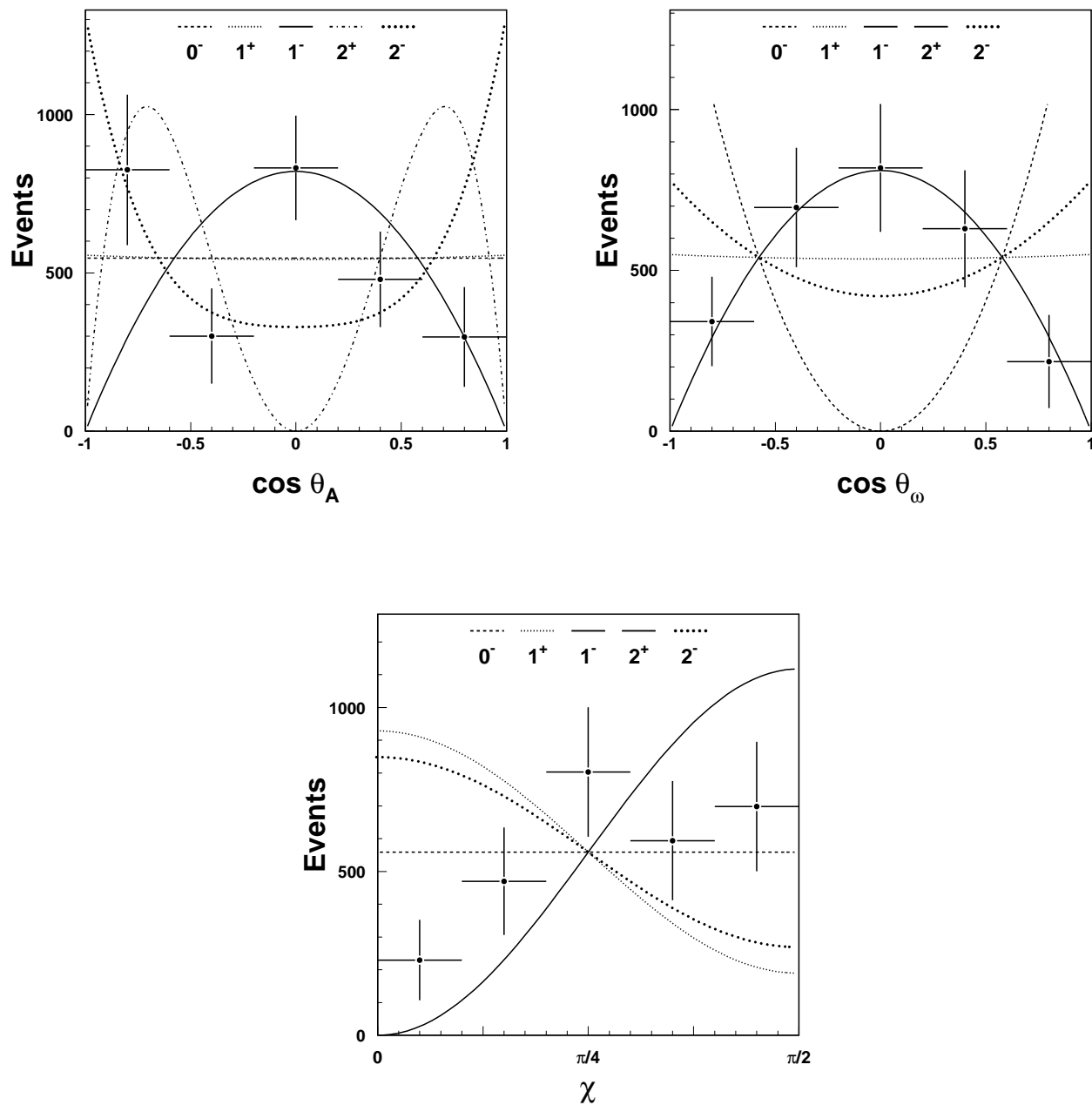


Figure 23: The angular distribution of θ_A (top-left), θ_ω (top-right) and χ (bottom). The curves show the best fits to the data for for different J^P assignments. (The 0^- and 1^+ are almost indistinguishable in $\cos \theta_A$, while the 1^- and 2^+ are indistinguishable in $\cos \theta_\omega$ and χ).

Table 7: Measured ρ' Mass and Width

Mode	Mass (MeV)	Width (MeV)
$B^0 \rightarrow D^{*+}\omega\pi^-$	1432 ± 37	376 ± 47
$B^- \rightarrow D^{*0}\omega\pi^-$	1367 ± 75	439 ± 135
$B \rightarrow D\omega\pi^-$	1415 ± 43	419 ± 110
Average	1418 ± 26	388 ± 41

Other possible changes in the mass and width are more difficult to evaluate. They include different Breit-Wigner parameterizations and the possibility of other resonant or non-resonant components in the $\omega\pi^-$ mass distributions.

Signals for $\omega\pi^-$ resonances have been detected before below 1500 MeV. There is a well established axial-vector state the $b_1(1235)$ with mass 1230 MeV and width 142 MeV. Data on vector states, excited ρ 's, is inconsistent. Clegg and Donnachie [11] have reviewed $\tau^- \rightarrow (4\pi)^-\bar{\nu}$, $e^+e^- \rightarrow \pi^+\pi^-$ and $e^+e^- \rightarrow \pi^+\pi^+\pi^-\pi^-$ data, including the $\omega\pi$ final state. Their best explanation is that of two 1^- states at 1463 ± 25 MeV and 1730 ± 30 MeV with widths 311 ± 62 and 400 ± 100 MeV, respectively. Only the lighter one decays into $\omega\pi$. The situation is quite complex, however. They conclude that these states must be mixed with non- $q\bar{q}$ states in order to explain their decays widths. There is also an observation of a wide, 300 MeV, $\omega\pi^0$ state in photoproduction at 1250 MeV [12], that is dominantly the $b_1(1235)$ [13] with possibly some 1^- in addition. Our state is consistent with the lower mass ρ' . We do not seem to be seeing significant production of the higher mass state into $\omega\pi^-$, as expected.

Several models predict the mass and decay widths of excited ρ and ω mesons. For example, according to Godfrey and Isgur [14] the first radial excitation of the ρ is at 1450 MeV. There is a large variation among the models, however, on prediction of the relative decays widths ranging from no $\pi\pi$ to $\pi\pi$ being equal to $\omega\pi$ [15].

Since we have observed a wide 1^- state in the mass region where the ρ' is expected, the most natural explanation is that we are observing the ρ' for the first time in B decays.

We note that τ^- lepton decays into $\omega\pi^-$ have been observed, and the 1^- spin-parity definitely established [16]. However, the relatively low mass of the τ^- distorts the the mass spectrum significantly, and makes it difficult to extract the ρ' mass and width [17].

9 Search For Other Resonant Substructure in $D^*(4\pi)^-$

We have accounted for $\sim 20\%$ of the $(4\pi)^-$ final state. We would like to disentangle other resonant substructure. Since the background is large in modes other than $D^0 \rightarrow K^-\pi^+$ we will only use this mode. One process that comes to mind is that where the virtual W^- materializes as an a_1^- , that subsequently decays into $\pi^+\pi^-\pi^-$ and we produce a D^{*++} that decays into $D^{*+}\pi^0$. This process should be the similar to that previously seen in the reaction $B^- \rightarrow D^{*0}\pi^-$, where the D^{*0} decayed into a $D^{*+}\pi^-$ [18]. We search for the presence of an a_1^- by examining the $\pi^+\pi^-\pi^-$ mass spectrum in Fig. 24.

There is an excess of signal events above background in the a_1^- mass region, that cannot be definitely associated with the a_1 . Proceeding by selecting events with $\pi^+\pi^-\pi^-$ masses between 0.6 and 1.6 GeV, we show the $D^{*+}\pi^0$ invariant mass spectrum in Fig. 25.

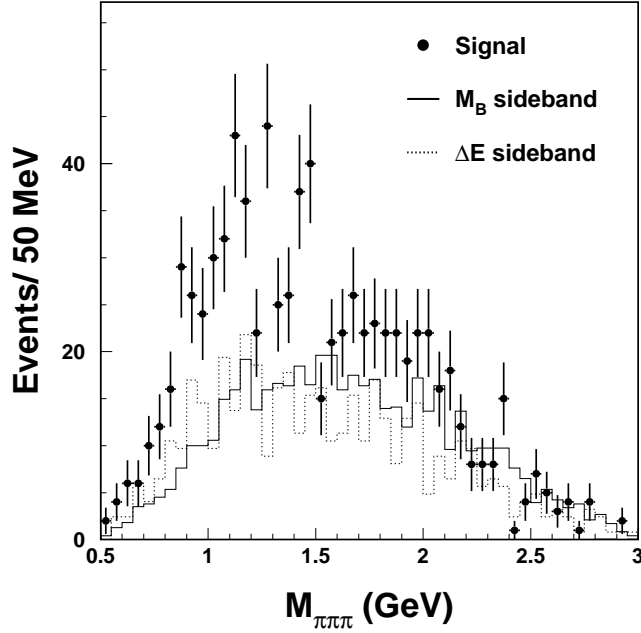


Figure 24: The invariant mass spectra of $\pi^+\pi^-\pi^-$ for the final state $D^{*+}\pi^+\pi^-\pi^-\pi^0$ for $D^0 \rightarrow K^-\pi^+$. The solid histogram is the background estimate from the M_B lower sideband and the dashed histogram is from the ΔE sidebands; both are normalized to the fitted number of background events.

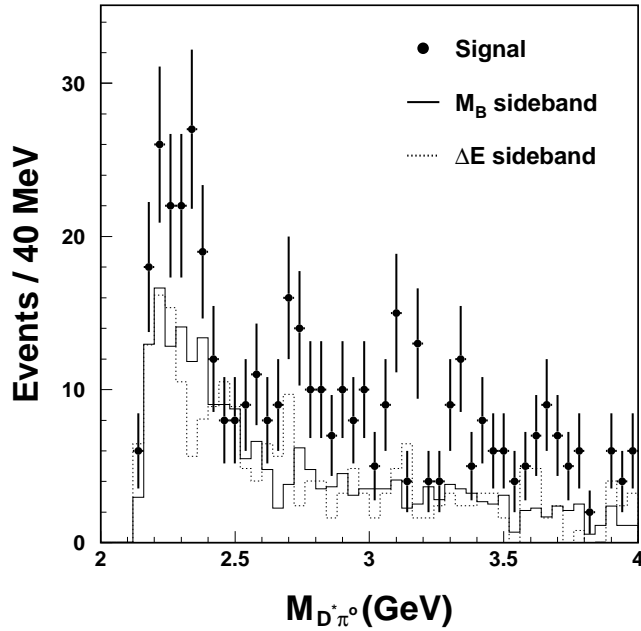


Figure 25: The invariant mass spectra of $D^{*+}\pi^0$ for $\pi^+\pi^-\pi^-$ masses between 0.6 - 1.6 GeV for the final state $D^{*+}\pi^+\pi^-\pi^-\pi^0$ with $D^0 \rightarrow K^-\pi^+$. The solid histogram is the background estimate from the M_B lower sideband and the dashed histogram is from the ΔE sidebands; both are normalized to the fitted number of background events.

Although there is a suggestion of a low mass enhancement, it is not consistent with D^{**} production that would peak in region of 2.42 - 2.46 GeV. Perhaps we are seeing an indication of fragmentation at the $b \rightarrow c$ decay vertex here.

We also display for completeness the “ $a_1^- \pi^0$ ” mass distribution in Fig. 26. There may or may not be a wide structure in the $(4\pi)^-$ mass. At this point we abandon our search for substructure in this decay channel.

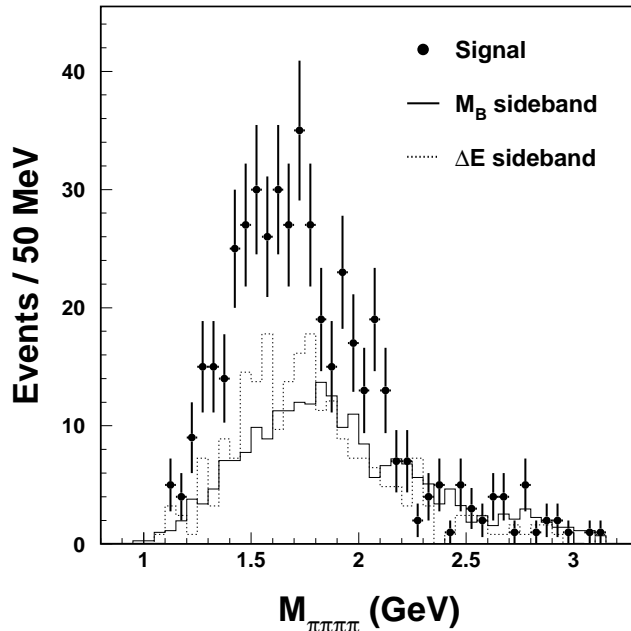


Figure 26: The invariant mass spectra of $\pi^+\pi^-\pi^-\pi^0$ for $\pi^+\pi^-\pi^-$ masses between 0.6 - 1.6 GeV for the final state $D^{*+}\pi^+\pi^-\pi^-\pi^0$ with $D^0 \rightarrow K^-\pi^+$. The solid histogram is the background estimate from the M_B lower sideband and the dashed histogram is from the ΔE sidebands; both are normalized to the fitted number of background events.

10 Conclusions

We have made the first statistically significant observations of six hadronic B decays shown in Table 8.

There is a low-mass resonant substructure in the $\omega\pi^-$ mass. A simple Breit-Wigner fit assuming a single resonance and no background gives a mass of $1418 \pm 26 \pm 19$ MeV with an intrinsic width of $382 \pm 41 \pm 32$ MeV.

The structure at 1418 MeV has a spin-parity consistent with 1^- . It is likely to be the elusive ρ' resonance [11]. These are by far the most accurate and least model dependent measurements of the ρ' parameters. The ρ' dominates the final state. (Thus the branching ratios for the $D^{(*)}\omega\pi^-$ apply also for $D^{(*)}\rho'^-$.)

Heavy quark symmetry predicts equal partial widths for $D^*\rho'$ and $D\rho'$. We measure the relative

Table 8: Measured Branching Ratios

Mode	\mathcal{B} (%)	# of events
$\overline{B}^0 \rightarrow D^{*+} \pi^+ \pi^- \pi^- \pi^0$	$1.72 \pm 0.14 \pm 0.24$	1230 ± 70
$\overline{B}^0 \rightarrow D^{*+} \omega \pi^-$	$0.29 \pm 0.03 \pm 0.04$	136 ± 15
$\overline{B}^0 \rightarrow D^+ \omega \pi^-$	$0.28 \pm 0.05 \pm 0.03$	91 ± 18
$B^- \rightarrow D^{*0} \pi^+ \pi^- \pi^- \pi^0$	$1.80 \pm 0.24 \pm 0.25$	195 ± 26
$B^- \rightarrow D^{*0} \omega \pi^-$	$0.45 \pm 0.10 \pm 0.07$	26 ± 6
$B^- \rightarrow D^0 \omega \pi^-$	$0.41 \pm 0.07 \pm 0.04$	88 ± 14

rates to be

$$\frac{\Gamma(\overline{B}^0 \rightarrow D^{*+} \rho'^-)}{\Gamma(\overline{B}^0 \rightarrow D^+ \rho'^-)} = 1.04 \pm 0.21 \pm 0.06 \quad (20)$$

$$\frac{\Gamma(B^- \rightarrow D^{*0} \rho'^-)}{\Gamma(B^- \rightarrow D^0 \rho'^-)} = 1.10 \pm 0.31 \pm 0.06 \quad (21)$$

$$\frac{\Gamma(B \rightarrow D^* \rho'^-)}{\Gamma(B \rightarrow D \rho'^-)} = 1.06 \pm 0.17 \pm 0.04 \quad . \quad (22)$$

Thus the prediction of heavy quark symmetry is satisfied within our errors.

Factorization predicts that the fraction of longitudinal polarization of the D^{*+} is the same as in the related semileptonic decay $B \rightarrow D^* \ell^- \bar{\nu}$ at four-momentum transfer q^2 equal to the mass-squared of the ρ'

$$\frac{\Gamma_L(B \rightarrow D^{*+} \rho'^-)}{\Gamma(B \rightarrow D^{*+} \rho'^-)} = \frac{\Gamma_L(B \rightarrow D^* \ell^- \bar{\nu})}{\Gamma(B \rightarrow D^* \ell^- \bar{\nu})} \Big|_{q^2=m_{\rho'}^2} \quad . \quad (23)$$

Our measurement of the D^{*+} polarization (see Fig. 14) is $(63 \pm 9)\%$. The model predictions in semileptonic decays for a q^2 of 2 GeV², are between 66.9 and 72.6% [19]. Thus this prediction of factorization is satisfied.

We can use factorization to estimate the product of the ρ' decay constant $f_{\rho'}$ and the branching ratio for $\rho'^- \rightarrow \omega \pi^-$. The relevant expression is

$$\frac{\Gamma(B \rightarrow D^{*+} \rho'^-, \rho'^- \rightarrow \omega \pi^-)}{\frac{d\Gamma}{dq^2}(B \rightarrow D^* \ell^- \bar{\nu})|_{q^2=m_{\rho'}^2}} = 6\pi^2 c_1^2 f_{\rho'}^2 \mathcal{B}(\rho'^- \rightarrow \omega \pi^-) |V_{ud}|^2 \quad , \quad (24)$$

where $f_{\rho'}$ is the so called ρ' decay constant and c_1 is a QCD correction factor. We use $c_1 = 1.1 \pm 0.1$ [20].

We use the semileptonic decay rates given in Barish *et al.* [21]. The product

$$f_{\rho'}^2 \mathcal{B}(\rho'^- \rightarrow \omega \pi^-) = 0.011 \pm 0.003 \text{ GeV}^2 \quad , \quad (25)$$

where the error is the quadrature of the experimental errors on the experimental branching ratios and c_1 .

The model of Godfrey and Isgur predicts decay constants widths and partial widths of mesons comprised of light quarks by using a relativistic treatment in the context of QCD [14]. They predict both $f_{\rho'}$ and $\mathcal{B}(\rho'^- \rightarrow \omega \pi^-)$; the values are 80 MeV and 39%, respectively. The branching ratio prediction is believed to be more accurate [22]. We use this to extract

$$f_{\rho'} = 167 \pm 23 \text{ MeV} \quad . \quad (26)$$

The model predicts a lower value for $f_{\rho'}$ observed here, if factorization is correct.

We note that all the $B \rightarrow D^{(*)}\rho'$ branching ratios that we have measured are approximately equal to the $B \rightarrow D^{(*)}\rho$ branching rates [4] if a model value of $\mathcal{B}(\rho'^- \rightarrow \omega\pi^-) = 39\%$ is used.

Finally, although the $\bar{B}^0 \rightarrow D^{*+}(4\pi)^-$ and $B^- \rightarrow D^{*0}(4\pi)^-$ branching ratios are nearly equal, the $\omega\pi^-$ branching ratios are about 1.5 times larger for the charged B than the neutral B , maintaining the trend seen for the π^- and ρ^- final states. Since the B^- lifetime is if anything longer than the B^0 , this trend must reverse for some final states. It has not for $D^{(*)}\rho'$.

11 Acknowledgements

We thank A. Donnachie, N. Isgur and J. Rosner for useful discussions. We gratefully acknowledge the effort of the CESR staff in providing us with excellent luminosity and running conditions. This work was supported by the National Science Foundation, the U.S. Department of Energy, the Research Corporation, the Natural Sciences and Engineering Research Council of Canada, the A.P. Sloan Foundation, the Swiss National Science Foundation, the Texas Advanced Research Program, and the Alexander von Humboldt Stiftung.

References

- [1] C. Caso *et al.*, The European Physical Journal **C3** (1998) 1.
- [2] G. Brandenburg *et al.* (CLEO), Phys. Rev. **D61**, 072002 (2000).
- [3] ARGUS previously reported a signal of 28 ± 10 events in this mode, corresponding to a branching ratio of $(3.4 \pm 1.8)\%$. H. Albrecht *et al.*, Z. Phys. **C 48**, 543 (1990).
- [4] M. Alam *et al.* (CLEO), Phys. Rev. **D 50**, 43 (1994); B. Barish *et al.* (CLEO), “Exclusive Reconstruction of $B \rightarrow D^{(*)}(n\pi)^-$ Decays,” CONF 97-01, EPS 339 (1997).
- [5] The CLEO II detector is described in Y. Kubota *et al.*, Nucl. Instrum. Methods A **320**, 66 (1992), and CLEO II.V in T. Hill, *ibid* A **418**, 32 (1998).
- [6] G. Fox and S. Wolfram, Phys. Rev. Lett. **23**, 1581 (1978).
- [7] We do not find significant differences between the CLEO II and II.V data sets.
- [8] We assume that $\omega\pi$ is in a 1^- final state. The difference between the 1^- efficiency and flat assumption is less than 2%.
- [9] M. Jacob and G.C. Wick, *Ann. Phys. (N.Y.)* **7** (1959) 404; J. D. Jackson, in *High Energy Physics, Les Houches, 1965*, Gordon and Breach, NY (1966); M.L. Perl, *High Energy Hadron Physics*, Wiley, NY (1974).
- [10] We allowed a systematic error of 5.5% on the number of events in each angular bin resulting possibly from the fitting procedure to the M_B spectrum. This changed the probability of χ^2 for the 1^- case to 3.9% from 3.8%, and negligible changes in the other cases.
- [11] A. B. Clegg and A. Donnachie, Z. Phys. **C 62**, 455 (1994).
- [12] D. Aston *et al.*, Nucl. Phys. **B234**, 1 (1984).

- [13] J. Brau *et al.*, Phys. Rev. **D37**, 2379 (1988).
- [14] S. Godfrey and N. Isgur, Phys. Rev. **D 32**, 189 (1985).
- [15] G. Busetto and N. Oliver, Z. Phys. **C 20** 247 (1983); R. Kokoski and N. Isgur, Phys. Rev. **D 35** 907 (1987).
- [16] K. Edwards *et al.* (CLEO), Phys. Rev. **D61** 072003 (2000).
- [17] The ρ' mass and width are also estimated from $\tau^- \rightarrow \pi^+ \pi^0 \nu_\tau$ decays, but the large interference from the $\rho(770)$ tail causes these results to have large uncertainties. See S. Anderson *et al.* (CLEO), Phys. Rev. **D61** 112002 (2000).
- [18] M. S. Alam *et al.* (CLEO), Phys. Rev. **50**, 43 (1994); S. Anderson *et al.* (CLEO), "Observation of a Broad $L = 1$ cq state in $B^- \rightarrow D^{*+} \pi^- \pi^-$ at CLEO," CONF 99-6 (1999).
- [19] N. Isgur and M. B. Wise, Phys. Lett. **B237**, 527 (1990); M. Wirbel *et al.*, Z. Phys. **C29**, 627 (1985); N. Neubert, Phys. Lett. **B264**, 455 (1991).
- [20] The error is due to the uncertainty in the scale where the Wilson coefficients are evaluated. See T. Browder, K. Honscheid and S. Playfer, "A Review of Hadronic and Rare B Decays," in *B Decays 2nd Edition*, ed. by S. Stone, World Scientific, Singapore (1994).
- [21] B. Barish *et al.* (CLEO), Phys. Rev. **D51** 1014 (1995). We correct for the new value of the $D^0 \rightarrow K^- \pi^+$ branching ratio.
- [22] Private communication from N. Isgur. The decay constants given in ref. [14] are dimensionless and must be multiplied by m to put them in the convention used here. An additional a factor of $\sqrt{2}$ must be used to convert from the electromagnetic form-factor to the weak form-factor using CVC.